DNA SIGNAL INDUCED FUSION AND AGGREGATION BEHAVIORS OF SYNTHETIC CELLS

by

Hengming Qiu

A Thesis

Submitted to the Faculty of Purdue University

In Partial Fulfillment of the Requirements for the degree of

Master of Science in Mechanical Engineering

School of Mechanical Engineering

West Lafayette, Indiana

December 2020

THE PURDUE UNIVERSITY GRADUATE SCHOOL
STATEMENT OF COMMITTEE APPROVAL

Dr. Jong Hyun Choi, Chair
School of Mechanical Engineering

Dr. Chengde Mao
Department of Chemistry

Dr. Bumsoo Han
School of Mechanical Engineering

Approved by:
Dr. Nicole Key

To my parents

ACKNOWLEDGMENTS

I would like to express my deepest gratitude to my master advisor, Professor Jong Hyun Choi, for his inspiration, encouragement, guidance, and financial support throughout my research. His passion, knowledge, energy, and commitment for research has been the greatest source of inspiration and strength for me. Professor Choi has served as a role model for me, and has helped me overcome different challenges and difficulties in my research over the years. Under his guidance and support, I gradually became an independent researcher. This very valuable experience of working with Professor Choi has helped build the confidence in me to face and take any challenges ahead, and will continue to be a source of inspiration and strength for me, and will guide me in my future career. I would also like to thank each and every committee member Professor Chengde Mao, and Professor Bumsoo Han for their kind advice and help in my research throughout my master study. I also acknowledge the support from the Office of Naval Research, the National Science Foundation, and the Department of Energy for their partial support of this work.

For the most time in my master study, I explored many issues and discussed about life and research topics with my laboratory mates. I have learned a lot from my peer mates. As both friends and colleagues, my laboratory teammates have been very helpful and wonderful and have provided lots of help to me. I would like to thank my fellow laboratory mates Dr. Jing Pan, Dr. Feiran Li, Ruixin Li, Yancheng Du, Jaehoon Ji for their help.

Last but not least, I would like to thank my parents for their support. They have always been encouraging and supportive. They trust in me and support me. They understand the difficult decisions I have made and have given their best to support me.

TABLE OF CONTENTS

LIST OF TABLES 7
LIST OF FIGURES 8
ABBREVIATIONS 13
ABSTRACT 14
1. INTRODUCTION 15
1.1 DNA Nanotechnology 16
1.1.1 DNA Origami 16
1.2 Lipids and Liposomes 17
1.3 Artificial Cells with DNA Nanotechnology 17
1.3.1 Artificial Cells with Origami Pores 17
1.3.2 Liposome Fusion Induced by DNA Signals 18
1.3.3 Liposome Aggregation Induced by DNA Signals 18
1.4 Motivation 19
1.5 Scope of the Study 19
1.6 Organization 19
2. METHODS 20
2.1 Materials 20
2.2 Liposome Preparation 20
2.2.1 Giant Unilamellar Vesicles 20
2.2.2 Small Unilamellar Vesicles 21
2.3 Characterization Methods 21
2.3.1 AFM Imaging 21
2.3.2 Spectral Characterization 22
2.3.3 Ensemble Fluorescence Measurement 22
2.3.4 Dynamic Light Scattering Measurement 22
2.3.5 Fluorescence Microscopy 22
2.4 Microfluidic Channel Assembly 23
2.5 Surface Passivation 23
3. LIPOSOME FUSION VIA DNA SIGNALS 24

3.1 Introduction 24
3.2 Scheme 25
3.3 Experimental Methods 26
3.3.1 Materials 26
3.3.2 Sample Preparation Methods 26
3.3.3 Characterization 26
3.3.4 Kinetic Measurement 28
3.4 Results and Discussion 29
3.5 Conclusion 33
4. PROGRAMMABLE AGGREGAGATION OF ARTIFICIAL CELLS WITH DNA SIGNALS 34
4.1 Introduction 34
4.2 Scheme 36
4.3 Experimental Methods 38
4.3.1 Materials 38
4.3.2 Sample Preparation Methods 40
4.3.3 Characterization 42
4.3.4 Kinetics 48
4.4 Results and Discussion 48
4.5 Conclusion 59
5. CONCLUSION AND FUTURE WORK 60
5.1 Conclusion 60
5.2 Future Work 60
REFERENCES 62
APPENDIX A. ORIGAMI SEQUENCE 66
VITA 72

LIST OF TABLES

Table 2.1. The lipids used in the experiments are listed. All the lipids used are purchased from Avanti Polar Inc. 20

Table 4.1. Sequences of DNA linker, releaser, and modified strands. The SUV linker can bind with both SUV and GUV strands, thereby connecting SUVs on a GUV. The hairpin strand includes the sequence of SUV linker which may be exposed after digestion of ACA TCT AAC AAC CAA ACC AT by Exo III. The GAA TCA part in the SUV linker is used as a toehold for the SUV releaser. In the cap releaser strand, AGT GCT GA is used as the toehold. Note that Cy5-DNA is a chimeric DNA/RNA oligonucleotide with rArU indicating RNA bases. 38

Table A.1. Blue and gray staple sequences for the origami tile shown in Figure 4.2. Colored parts correspond to the colored dots in Figure 4.2. For example, staple [02,08] in Figure 4.2a has a red dot. In this table, there is a red '/5Cy5/' at the 5' end of the staple's sequence. Similar notations apply to pink (pore-cap connection) and green (cap-pore connection) colored parts. For the staple without a colored dot, colored parts will not show up in the sequence. This means that staple [02,08] in Figure 4.2b does not have '/5Cy5/' at the 5' end. 66

Table A.2. Red staple sequences for the origami tile shown in Figure 4.2. Sky-blue parts correspond to the sky-blue dots in Figure 4.2. For example, staple [02,16] in Figure 4.2a has a sky-blue dot. In this table, there is a sky-blue extension at the 3' end of the staple's sequence. All the sky-blue extensions are designed to bind with a cholesterol-DNA, whose sequence is TGGACGGCCGTCAACTGCGGCGTGTAA/3CholTEG/. For the staple without a sky-blue dot, colored parts will not show up in the sequence. This means, for example, that staple [02,16] in Figure 4.2b does not have the blue extension at the 3' end. 70

Table A.3. Sequence of tubular staples. These staples are designed to bind the upper and lower boundaries of the origami tile together, thus forming a tubular pore. 71

LIST OF FIGURES

Figure 3.1. Schematic for liposome fusion induced by DNA signals (a) Small liposome encapsulated SRB and has linker strand on its surface is immobilized in glass surface with non-specific binding (b) Another type of small liposome with no SRB encapsulated and linker strand complimentary with the first one is introduced into the channel. (c) When two liposome collide, the complimentary DNA strands on adjacent liposome hybridized (d) The hybridization of membrane anchored DNA strand exert force to the adjacent membranes and induced liposome fusion..... 25

Figure 3.2. DLS measurement of SUV-A, SUV-B, and SUV-A and SUV-B mixed at 1 to 1 ratio at 20°C, 37°C, 50°C for 1 hour. The mixture at 20°C, 37°C, 50°C has an 49%, 98%, 108% increase in average hydrodynamic diameter respectively..... 27

Figure 3.3. SUV encapsulated with different concentration of SRB. Fluorescence intensity changed more from 10mM to 5mM than from 15mM to 10mM. Therefore, we choose to encapsulate 10mM SRB in SUV..... 28

Figure 3.4. SUV kinetic fluorescence measurement. (a) Kinetic fluorescence measurement of SUV-A (encapsulated with SRB) only and SUV-A mixed with SUV-13w (uncomplimentary DNA strand) does not show significant increase of intensity at 582nm. Kinetic fluorescence measurement of SUV-A mixed with SUV-B shows 30% increase of fluorescence intensity in 1-hour period. (b) Fluorescence intensity increase with regard to SUV-A only (c) Control experiment, fluorescence intensity of DI water, 10mM Mg^{2+} PBS buffer, SUV-A, SUV-B, SUV-13w, SUV-A mixed with SUV-13w (at 0 min), SUV-A mixed with SUV-B (at 0 min). 29

Figure 3.5. Single case study of lipid fusion in fluid channel at room temperature. (a,b,c)SUV with SRB was first flow into the fluid channel, and some of them are non-specifically bind on the coverslip. Then SUV with complimentary DNA strand is flow into the channel. Once the two types of SUV attached, the fluorescence intensity of SRB probe raise, indicating that the two overlapped SUV are fused. (d) SUV with uncomplimentary DNA strand does not overlap, and therefore we do not observe fluorescence increase..... 30

Figure 3.6. Temperature effect on liposome fusion. (a) 16% overlap of liposome with complimentary DNA strand incubate at 20°C for 1 hour. (b) 50% overlap of liposome with complimentary DNA strand incubate at 37°C for 1 hour.(c) 65% overlap of liposome with complimentary DNA strand incubate at 50°C for 1 hour. (d) 11% overlap of liposome with uncomplimentary DNA strand incubate at 20°C for 1 hour. (e) 17% overlap of liposome with uncomplimentary DNA strand incubate at 37°C for 1 hour. (f) 21% overlap of liposome with uncomplimentary DNA strand incubate at 50°C for 1 hour. (g) Overlap ratio in histogram 32

Figure 4.1. Scheme for reversible cell aggregation programmed by DNA signals. (a) By biotin-streptavidin conjugation, a giant vesicle is immobilized on a BSA modified glass surface. The GUV has DNA strands (shown in blue), has DNA origami tubule (orange) transmembrane channels, and encapsulates Exo III on a polystyrene particle (yellow-red). (b) The pores are initially closed with flat origami caps which can be removed by toehold-mediated strand displacement by 'cap-releaser' strands. (c) Via the membrane channels, an external DNA hairpin

signal may reach the vesicle where it is transduced by Exo III into another type of signal through enzymatic reaction. The enzyme digests a portion of the hairpin from the 3 end, exposing the complementary domains on the vesicles for the strands (both blue and red). (d) Processed signaling oligonucleotides pass through the pores of the origami and cause several small vesicles to accumulate on the GUV. (e) By removing the linker strands, another DNA signal, 'SUV releaser' strands shown in pink, can dissociate the SUVs attached to the giant vesicle. It is possible to program this association and dissociation activity with DNA signals and continuously indefinitely in principle. 36

Figure 4.2. The origami designs and folding path diagrams for the tubular pore (a) and rectangular cap (b). (a) The 32-helix origami tile (identical in both (a) and (b)) before cyclization to form the tubular pore (see Table A.1 and A.2 for staples). A set of staples (termed tubular staples) are used to connect the top and bottom of the tile, forming a tubule (see Table A.3). The tubular staples are not shown in the schematic. A Cy5-DNA strand used for fluorescence imaging, shown in Figure 2a-b, is marked in red. A total of 30 staple strands (15 on each side) are added a 16-nt extension to connect the pore with the cap. The 15 staples marked in sky-blue are designed to link with cholesterol-DNA with a 27-nt extension (see Table A.2). (b) The rectangular origami cap. Each of 10 staples (indicated by green dots) have a 24-nt extension on 5' end: 16-nt (TTCGGACAGAGTGACA) for binding the pore, and 8-nt (AGTGCTGA) for toehold. (c) Schematic of the tubular pore closed with the rectangular cap. The sky-blue stripe represents the cholesterol moieties. The pink and green denote the staple extensions for capping. 39

Figure 4.3. AFM images of DNA origami. (a) Near 100% flat origami rectangles, which measure approximately 60 nm x 100 nm in dimension. (b) The majority of DNA origami measures approximately 60 nm x 50 nm with a thickness of ~4 nm, which is roughly half the size and twice the thickness of the origami rectangle. The results indicate the identity of the tubular structure of the origami in solution, which should have a diameter of ~32 nm and a length of ~60 nm. Note that the tubular structures collapsed into a rectangular shape to maximize their contact with the mica substrate. (c) Origami structures after connecting tubules with tiles at a ratio of 1: 2. Most tubules are connected to flat tiles, while the linked origami structures in 3D collapsed before or during the AFM imaging. (d) Zoom-in of the black square area in (c). The scale bar is 20 nm. Colored lines (blue, red, and pink) denote the sites where heights are measured. (e) Corresponding height profiles of the objects in (d). Cross-sections of a flat tile (blue), an isolated tubule (red), and a tubule connected with a flat tile (pink). Dashed line indicates the mica substrate. The profiles confirm the connection between the tubule and flat tile. (f) Origami tiles and tubules after mixing with cap releaser strands. The majority (~90%) of the tubules are separate from the tiles, suggesting that cap releasers are effective in removing the flat caps from the tubules. 43

Figure 4.4. Exo III activity measured with a FAM-quencher pair in solution. (a) Fluorescence measurement with free Exo III enzymes. Initially, fluorescence is measured from 1 μM of FAM-DNA in solution. Upon addition of quencher-cDNA at 1 μM (black arrow), the fluorescence intensity immediately drops. After a few minutes, we added 1 nM Exo III enzymes into the solution (red arrow), which results in the increase of fluorescence intensity. (b) Fluorescence measurement in a similar experiment with particle-Exo III rather than free enzymes. The addition of polystyrene particle modified Exo III enzymes into the solution of FAM-DNA and cDNA-quencher (1 μM each; green arrow) leads to the increase of fluorescence intensity. (c)-(d) Fluorescence measurement with enzyme-particles encapsulated in giant vesicles with open origami pores. Black Arrow indicate the addition of cDNA-quencher into the solution of FAM-DNA (1 μM each). Then,

GUVs containing enzyme-particles are added to the solution (blue arrow). A small, yet distinct increase of the fluorescence intensity is observed. After a few minutes, particle-Exo III (without vesicles) are added directly to the solution (green arrow), which results in a further increase of the fluorescence intensity. 46

Figure 4.5. AFM image of DNA origami tiles after incubation with Exo III. Approximately 10 nM DNA origami tiles were mixed with 0.1 nM Exo III enzymes in 10 µL TAEM buffer for 15 mins. The AFM image shows that most of the rectangular origami remains its original shape, indicating that this concentration of Exo III will do little damage to the origami. 47

Figure 4.6. Shape change of a GUV during a one-hour period. Scale bar: 5 µm. 47

Figure 4.7. Brightfield (left) and fluorescence (right) images of giant vesicles. GFP is shown in a green color in fluorescence images and Cy5 is shown in red. (a) DNA tubules modified by cholesterol may be integrated into the vesicle membrane. A distinct, ring-shaped fluorescence pattern around the vesicle boundary is shown by the Cy5 functionalized origami. (b) Origami DNA cannot be injected into the membrane without cholesterol moieties, so no fluorescence is observed. (c) via transmembrane channels made of tubular origami, GFP can penetrate into the vesicle. (d) GFP cannot disperse into the vesicle without DNA tubules. (e) With DNA pores, Cy5-DNA may join the vesicle. (f) When no origami pores are present on the surface of the vesicle, the fluorophore-labeled DNA cannot pass into the GUV. Notice that with Cy5 dyes, the origami tubules in (c and e) are not functionalized. Scale bars are 5 µm. 49

Figure 4.8. Kinetic measurement of molecular outflux through origami pores from giant vesicles immobilized on the glass coverslip surface. (a) Fluorescence images of GFP molecules (shown in pink color) overlaid with brightfield images of a vesicle at time t = 0 and 60 min. The molecules, initially encapsulated in the GUV, diffuse out of the vesicle after the pores are opened. (b) The fluorescence intensity inside the vesicle decreases, shortly after the cap-releaser strands were introduced into the microfluidic imaging chamber (indicated by the orange arrow). The exponential curve-fit (orange line) suggests a time constant of ~3 min. (c) Fluorescence images of Cy5-DNA inside a giant vesicle overlaid with brightfield images at time t = 0 and 90 min. (d) The fluorescence diminishes after adding the cap releasers (orange arrow) with a ~8-min time constant. Scale bars are 5 µm. 50

Figure 4.9. Kinetic measurements of molecular transport through DNA origami pores. (a) Fluorescence images of GFP molecules initially encapsulated inside a GUV at the beginning (t = 0 min) and end (t = 90 min) of the experiment. (b) Normalized fluorescence intensity of GFP as a function of time. After 25 mins, the cap releaser strands were introduced to the imaging chamber to remove the origami caps and open the channels, as indicated by the black arrow. Shortly after that, the fluorescent molecules diffused out of the GUV, and the fluorescence intensity inside GUV dropped. (c)-(d) Control experiment with the GUV containing GFP, but without origami pores. The fluorescence intensity does not change significantly, indicating that no molecular transport in and out of the vesicle without pores. (e)-(f) Fluorescence measurement of Cy5-DNA encapsulated inside a giant vesicle over time. Fluorescence images at the beginning and end of the experiment (t = 0 and 90 min, respectively). Shortly after adding cap releaser strands (black arrow), the fluorescence intensity inside the GUV dropped. (g)-(h) Control experiment with the GUV encapsulating Cy5-DNA without origami channels. The fluorescence intensity remains constant over time without origami pores. 52

Figure 4.10. Reversible vesicle aggregation with DNA signals. (a) Fluorescence intensity of the small vesicles around the GUV on each experimental step. Corresponding images of fluorescence overlaid on brightfield images are also presented. Oligonucleotides (red strands in Figure 1) and rhodamine B dyes are present in the SUVs for imaging. On its surface, the giant vesicle includes DNA strands (blue strands in Figure 1), but does not have DNA origami pores or particles of polystyrene. (i) A giant vesicle is immobilized through biotin-streptavidin conjugation in the microfluidic imaging chamber. (ii) The introduction of small vesicles and 36-nt SUV-linker DNA (indicated by the red arrow) will cause SUV clustering on the giant vesicle through the base pairing of the giant and small vesicle linkers with the strands. The fluorescence intensity increases significantly as a result. (iii) A collection of SUV release strands, represented by a black arrow, is given. First the signaling oligonucleotides can bind with the 6-nt toehold and completely hybridize with the SUV-linkers, thus eliminating the vesicle linkers. Thus the tiny vesicles can dissociate from the GUV, and the strength of fluorescence decreases dramatically. (iv)—The (vii). With DNA signals, you can repeat the reversible vesicle aggregation (SUV linkers and releasers). (b) Control experiment, using a random sequence of DNA rather than the SUV linkers (represented by the blue arrows). As predicted, the small vesicles are not attached to the GUV, so no major fluorescence changes have been observed. Scale bars are 5 μm in all images. 54

Figure 4.11. (a) Dynamic aggregation behavior of artificial cells programmed by Hairpin signals. To receive and transmit signals, tubular origami pores are included in the giant vesicle which also encapsulates Exo-III modified polystyrene particles. The 200-nm-diameter particles, seen in the upper left image as yellow dots, float randomly within the GUV. I In the imaging chamber, a giant vesicle is immobilized. (ii) To remove the flat origami caps, a collection of cap releaser strands are given (orange arrow). (iii) As the red arrow shows, the hairpin strands and small vesicles are added to the tube. The hairpins penetrate through the transmembrane origami channels into the vesicle and are partially digested by Exo III, revealing the domain of the SUV linker. On the small and large vesicles, the transduced oligonucleotides diffuse out through the pores and bind with the strands. As a result, the tiny vesicles cluster around the surface of the GUV, which is apparent with a circular fluorescent image superimposed on the giant vesicle's bright field image. (iv) When the SUV releasers (represented by the black arrow) are inserted, the SUV linkers are removed by means of a toehold-mediated displacement of the strand. Then the tiny vesicles dissociate from the GUV, and the intensity of the fluorescence decreases dramatically. (v)-(viii) You can replicate the programmable clustering action of DNA many times. (b) Use a random series instead of a hairpin to monitor the experiment. (i)-(ii) The opening of the DNA pores is achieved by removing the caps (indicated by the orange arrow). (iii) Random sequence oligonucleotides may join the giant vesicle (blue arrow), but they are unable to cause small vesicle aggregation at the GUV. Therefore, no major fluorescence variations have been observed (iii). (iv) No modifications in the actions of the vesicles would result from the addition of SUV releasers. Scale bars are 5 μm in all images. ... 56

Figure 4.12. Additional reversible aggregation experiment with 2 cycles of adding SUVs, hairpin strands, and SUV releasers. For each step, we kept 1-hour incubation time, because the change of fluorescence intensity gradually stopped after 40 to 50 mins. Similar to Figure 5, yellow dots in the top left image represents polystyrene particles functionalized with Exo III enzymes. Circular fluorescence ring indicates the aggregation of small vesicles on the surface of the giant vesicle. 57

Figure 4.13. Additional aggregation experiment with hairpin signals. Significant changes of fluorescence intensity were observed during the course of experiment. It is noticeable that the

GUV immobilized on the glass surface gradually changed its shape from a sphere to ellipsoid. We suspect that this might be caused by the flow in the microfluidic channel..... 58

Figure 4.14. Control experiment without cap releaser strands. Small vesicles and hairpin strands were introduced into the microfluidic imaging chamber where a giant vesicle was immobilized with DNA pores closed with origami caps. Without adding cap releaser strands, the origami channels on the GUV remained closed; therefore, hairpin strands could not enter the GUV to become active SUV linker strand. As a result, we did not observe significant SUV binding on the GUV. There is only one spot that has nonspecifically bound SUV which was not removed by the SUV releaser strand. 59

ABBREVIATIONS

SUV	Small unilamellar vesicle
GUV	Giant unilamellar vesicle
MW	Molecular weight
SRB	Sulforhodamine B
GFP	Green fluorescent protein
EDTA	Ethylenediaminetetraacetic acid
TAEM	A buffer with 40 mM Tris, 20 mM acetiv acid. 1 mM EDTA and 12.5 mM Mg^{2+}
ORG	Origami
SNARE	Soluble *N*-ethylmaleimide-sensitive-factor attachment protein receptor

ABSTRACT

This thesis investigates the use of engineered DNA to program fusion and aggregation behaviors of artificial cells, mimicking biological cells and their important functions. To achieve this goal, we construct synthetic cells from engineered lipids and DNA to recognize and process intercellular signals.

Cell fusion is regulated by snap receptor (SNARE) proteins in mammalian cells. The zippering of SNARE proteins exerts forces to the adjacent cell membrane and induces membrane fusion. The hybridization of membrane anchored DNA can induce fusion in a similar way. The advantage of using DNA as a fusion signal is that oligonucleotides are much easier to engineer and control. In this study, we construct two types of small vesicles decorated with DNA oligonucleotides and demonstrate their fusion using programmable DNA base-pairing. Fluorescent probes are used to measure fusion events. The experiment advances our understanding of the dynamic vesicle fusion behavior.

Cell aggregation is a complex behavior that is closely associated to the differentiation, migration, and viability of biological cells. An effort to create synthetic analogs could lead to considerable advances in cell physiology and biophysics. Rendering and modulating such a dynamic artificial cell system require mechanisms for receiving, transducing, and transmitting intercellular signals, yet effective tools are limited at present. Here we construct synthetic cells and show their programmable aggregation behaviors using DNA oligonucleotides as a signaling molecule. The synthetic cells have transmembrane DNA origami that are used to recognize and process intercellular signals. We demonstrate that multiple small vesicles aggregate onto a giant vesicle after a transduction of external DNA signals by an intracellular enzyme, and that the small vesicles dissociate when receiving ‘release’ signals.

We envision that this thesis will provide a new platform for building programmable synthetic protocells capable of chemical communication and coordination.

1. INTRODUCTION

Nanotechnology has been studied since the last century, where numerous scientists have contributed to this field. It bloomed so fast in the past few decades that extensive new materials and characterization methods have been developed. As nanotechnology develops further, its application in biology and medicine has become more and more critical. Scientists can access and manipulate those tiny biological components, which can only be studied ensemble before. Thus, bio-nanotechnology which uses those biomaterials from life as its fundamental materials become popular, like proteins and DNA. Deoxyribonucleic acid, DNA, as one of the most essential biomaterials has attracted significant attention from researchers. Instead of using it as a genetic information carrier, DNA is used as an engineering material to build nanostructures and communicate between different systems. Protein is another big portion of bio-materials. While its function is highly dependent on a protein's sequence and structure, diverse studies can be done on proteins. Among all these proteins, motor protein is a type of essential proteins in vivo which controls the intracellular transport. This makes the motor proteins related to numerous diseases and necessary to be studied. However, given the complexity of the natural cell system, it is extremely difficult to understand all its details. Thus, the artificial cell was developed to study the problem. As the same lipid bilayer as natural cell, artificial cell has a much simpler internal environment and could be designed to have certain functions. This thesis presents the engineering of DNA signals, including their generation, process, and interaction with other DNA molecules, proteins, nanoparticles, and artificial cells. These studies explore the possibilities to extend the use of DNA as a signal to control artificial cell behavior.

This chapter introduces the recent progress in DNA nanotechnology and artificial cell research and the interaction between these materials. Our research effort in using DNA signals for artificial cell control is summarized in the scope of this study. The organization of the entire thesis is also presented.

1.1 DNA Nanotechnology

DNA is the most essential material that carries genetic information. It is a high molecular weight (MW) molecule composed of two polynucleotide chains that coil around each other to form a double helix. This ability comes from the Watson-Crick complementary principle in DNA structure. There are 4 types of nitrogenous bases in a DNA molecule, purine adenine (A), purine guanine (G), pyrimidine cytosine (C), and pyrimidine thymine (T). Among these four bases, A pairs with T and G pairs with C, each pair of bases forms hydrogen bonds which lower the free energy of the molecule and stabilize DNA double helix structure. With the base-pairing property, the assemble and disassemble of DNA strands could be controlled. Since each base pair is unique, the precision of control could be as high as the nanometer level. Thus DNA has been widely used in nanotechnology research.[1,2] It could be used as an engineering material to be assembled into larger-scale structures, which could be two-dimensional (2D) or even three-dimensional (3D). Furthermore, the whole functional structure could also interact with other molecules to achieve more applications including molecular probing, material deposition, drug delivery and more. This makes DNA a promising tool for nanotechnology research. Within DNA nanotechnology, DNA origami and DNA walker are all important nanostructures.

1.1.1 DNA Origami

DNA has become one of the most extensively used molecular building blocks for engineering self-assembling materials.[3] DNA origami is a technique used to fold a long single-stranded DNA, which is called a scaffold strand, into different designer nanoscale architectures using hundreds of short DNA oligonucleotides, called staple strands. The complexity and scalability of DNA nanostructures have significantly enhanced DNA origami. DNA origami has dramatically improved the complexity and scalability of DNA nanostructures.[4] Due to its high degree of customization and spatial addressability, DNA origami provides a versatile platform to engineer nanoscale structures and devices that can sense, compute, and actuate. These capabilities open up possibilities for a wide range of applications in chemistry, biology, physics, materials science and computer science, often involving programmed spatial control of 3D space molecules and atoms.

1.2 Lipids and Liposomes

Since the biological environment is very complicated, it is difficult to understand a cell's behavior as there are so many components inside. The artificial cell is needed to simplify the cellular environment to specifically study the interested factors and eliminate variations of other factors. The idea of artificial cell was first proposed by Dr. Thomas Ming Swi Chang in 1957.[5] Artificial cell is a substitute of the actual cell created by scientists. Different cell functions can be achieved in the artificial cell by adding components from a real biological cell. Thus it becomes a perfect tool to study cell behavior as all factors could be under control with this setup. Also, based on its similarity to biological cells, artificial cells could also be used in drug delivery or medical imaging. More importantly, since these synthetic cells can be created with functions different from natural cells, artificial cell research could also be considered as upgrading biological cells by inserting desired functions. All these factors make artificial cells attract lots of attention from scientists.

1.3 Artificial Cells with DNA Nanotechnology

Artificial cells can be prepared by different methods including the top-down and bottom-up approaches. One of these two methods can be chosen based on the complexity of the target system for study. The top-down approach starts from a real cell and reduces its components by editing the genes inside.[6] Bottom-up approach starts from an empty cell whose membrane is made by polymers, proteins, lipids or mixtures of these and gradually encapsulates needed cell components into the cell.[7] Among these materials, the lipid bilayer is the actual form of membrane for biological cell; thus lipids have been studied extensively.

1.3.1 Artificial Cells with Origami Pores

Transmembrane channels are crucial for a cell since they connect the inner cell environment with external biological conditions. They can select if certain molecules could have access to the inner space of the cells. With this function, successful control of cell transmembrane channels could become a substantial advantage for programming cell behaviors. Since large protein complexes are the common material for these channels, the study and control of these biomolecules are limited. Thus, instead of using proteins, DNA molecules have been proposed to construct transmembrane channels.[8,9] As mentioned in chapter 1.1, DNA can be assembled into 2D structure

and further into 3D. In addition, DNA could also be easily chemical modified and affected by external signals including light, pH, and enzymes. These abilities make DNA a perfect candidate for the transmembrane channel as it can be built into a similar shape and added more control possibilities.

1.3.2 Liposome Fusion Induced by DNA Signals

In nature, the fusion of phospholipid vesicles is regulated and catalyzed by highly specialized SNARE proteins.[10] During membrane fusion, v-SNARE and t-SNARE proteins on separate membranes combine to form a trans-SNARE complex. In this zipping process, it exerted force on the adjacent cell membranes and caused them to fuse. Inspired by nature's use of molecular recognition between receptor proteins, membrane-anchored DNA strands that are complementary have been used to force bilayers into proximity by the hybridization of complimentary DNA strands. This forced bilayer contact triggers vesicle fusion.

1.3.3 Liposome Aggregation Induced by DNA Signals

Cell aggregation is an important phenomenon in cellular biology where cells bind and cluster together under a certain environment.[11] Studying the cell-cell interactions during this process could contribute extensively to understanding cell differentiation, migration, and viability.[12-14] Furthermore, cell aggregation study also holds great potential in enhancing tissue engineering research as cell interactions are an essential part of tissue building.[15] Tissue engineering requires scaffold matrices that provide structural support and cellular signals to provide growth factor.[16] With this importance, plenty of research has been done on this topic, including the function of certain molecules associated, the kinetics and dynamics of cell aggregation and the possible diseases related to cell aggregation.[17] These works characterize cell aggregation behavior from all different aspects. However, given the complex inner cellular environment, to take full control of cellular aggregation and dissociation is difficult. Therefore, the simplified synthetic cell could be introduced to the system either for a deeper understanding of cell interaction or for better control of cell aggregation behavior. Synthetic cells include cell-like structure that has certain characteristics of living cells and can also be engineering materials that mimic some properties of cell, such as surface characteristics.

1.4 Motivation

The study of cellular environment is a very important topic as it is directly related to life. However, with its extreme complexity, simplification of this system is necessary in order to study. As one of the most popular and promising methods, artificial cell research shows its great importance. In order to achieve the similar cell functions inside a human-built lipid bilayer, the components of an artificial cell should be as close as possible to a real cell while they can be controlled by external signals. Transmembrane protein channels as the gate of cell help maintain the inner environment of cell. If a similar channel structure could also be implemented onto an artificial cell, the simulation of the real cell could take a big step forward. As one of the promising candidates for synthetic transmembrane channels, DNA origami pore research is still in its early stage. Much research needs to be performed on this topic, which has been the motivation of this thesis.

1.5 Scope of the Study

This thesis focuses on the interaction between synthetic cells and DNA nanotechnology. By using DNA signals, we study lipid fusion and aggregation behaviors.

1.6 Organization

This thesis discusses experimental efforts in using the DNA nanotechnology method to study synthetic cells. Chapter 2 provides the general experimental setups, sample preparation methods, and characterizations. The design and investigation of DNA induced synthetic cell fusion are presented in Chapter 3. The integration of DNA signals into artificial cells for reversible liposome aggregation and release are discussed in Chapter 4. Concluding remarks and future work are presented in Chapter 5.

2. METHODS

2.1 Materials

All the sequences were designed by us, purchased from Integrated DNA Technologies Inc and used without further purification. All the lipids used are purchased from Avanti Polar Inc. If not specified, other chemicals are purchased from Sigma-Aldrich.

Lipid information

Table 2.1. The lipids used in the experiments are listed. All the lipids used are purchased from Avanti Polar Inc.

Lipid in small vesicles	
16:0 PC or DPPC:	1,2-dipalmitoyl-sn-glycero-3-phosphocholine
16:0 Liss Rhod PE:	1,2-dipalmitoyl-sn-glycero-3-phosphoethanolamine-N-(lissamine rhodamine B sulfonyl) (ammonium salt)
Lipid in giant vesicles	
14:0 PC or DMPC	1,2-dimyristoyl-sn-glycero-3-phosphocholine
18:1 Biotinyl PE	1,2-dioleoyl-sn-glycero-3-phosphoethanolamine-N-(biotinyl) (sodium salt)
DSPE-PEG(2000)-DBCO	1,2-distearoyl-sn-glycero-3-phosphoethanolamine-N-[dibenzocyclooctyl(PEG)-2000]

2.2 Liposome Preparation

2.2.1 Giant Unilamellar Vesicles

Giant unilamellar vesicles (GUVs) are synthesized with inverted emulsion method[18] and used in lipid aggregation experiment. Approximately 10 mg/ml 1,2- dimyristoyl-sn-glycerol-3-phosphocholine (DMPC) and 1,2-Dioleoyl-sn-Glycero-3-Phosphoethanolamine-N-(Biotinyl) (18:1 Biotinyl PE) were mixed at 1:1 ratio to make a 100 μL solution. The mixed solution was added to a glass vial and dried in vacuum for 40 minutes to form a thin layer of lipid on the bottom of the glass vial. Then 600 μL liquid paraffin was added to the glass vial to dissolve the lipids. The glass vial is sealed and sonicated at 50 °C for 3 hours to have lipid disperse uniformly in the solution. To make liposome with nothing encapsulated, 20 μL of TAEM buffer (TAE buffer with 12.5 mM Mg^{2+}) was added to the mixture and vortexed for 20 s. To make liposome with Exo III

encapsulated inside and origami pore on the membrane, 10 μL 10 nM DNA origami tubules, 5 μL Exo III-particle, both in 1× TAEM were mixed and additional TAEM buffer added to adjust the volume of the mixture to 20 μL. The solution became turbid after vortex. The mixture was then pipetted on top of 300 μL TAEM buffer and placed in 4 °C refrigerator for 15 minutes and then centrifuged for 15 minutes at 8,000 g. After centrifuge, remove the oil solution above the TAEM solution, and the liposome is dissolved in the TAEM solution. From the molar ratio of components, we estimate that about 3,000,000 DNA-lipid conjugates integrated on the surface of each giant vesicle.

2.2.2 Small Unilamellar Vesicles

Small unilamellar vesicles (SUVs) are synthesized with rehydration method[19] and used in both vesicle fusion and lipid aggregation experiments. In both experiments, cholesterol modified DNA was mixed with 1,2-dipalmitoyl-sn-glycero-3-phosphocholine (DPPC) and 1,2-dipalmitoyl-sn-glycero-3-phosphoethanolamine (16:0 PE) at a molar ratio of 1:500:500 in a glass vial. To label SUV with DiD or Rhodamine B fluorescent dye, we added 1 μL dye solution to the mixed solution. The solution was dried in vacuum for 20 minutes. Then 1 mL preheated PBS solution at 90 °C was added to the glass vial. The solution was stirred by a stirring bar at 500 rpm for 1 hour on a hot plate of ~90 °C. To label SUV with SRB, add 10 mM SRB in preheated PBS solution. After stirring, SUV is purified by a 30 kDa molecular weight cut off spin column at 5,000 g for 5 minutes 6 times to remove free lipid molecules, free fluorophores, and free DNA oligonucleotides. From the molar ratio of components, we estimate roughly 50 oligonucleotides per small vesicle.

2.3 Characterization Methods

2.3.1 AFM Imaging

Atomic force microscopy (AFM) is used to characterize origami in lipid aggregation experiments. The origami solution was diluted to 1 nM by 1x TAEM buffer. Approximately 10 μL of the diluted solution was deposited on a freshly cleaved mica and incubation for 10 minutes. Then the solution was blown away with compressed air. To further rinsed the surface, we added 500 μL of DI water on the mica, and blown away with compressed air. The AFM imaging was performed with a SCANASYST-AIR probe.

2.3.2 Spectral Characterization

Absorption is a great way to determine the concentration of a molecule in solution quantitatively. A Perkin Elmer Lambda 950 spectrophotometer was used to measure the absorption spectra. Before measuring the sample, two cuvettes were first loaded with the 150 μL of solvent, and calibrated for the desired wavelength range. Then, we replaced the sample cuvette with a sample solution and performed the measurement. The concentration of molecules can be calculated with the absorption and the molar extinction coefficient.

2.3.3 Ensemble Fluorescence Measurement

Ensemble fluorescence measurement was used in vesicle fusion experiment by detecting the change of SRB concentration. A Horiba Fluorometer was used to perform measurements. A diluted sample was added to a cuvette and placed inside the instrument. After setting excitation wavelength, emission wavelength range and slit size, emission of the sample can be measured. In addition, this fluorometer can also be used to conduct kinetic measurements. With fixed excitation and emission wavelength set, the change of fluorescence intensity could be detected as a function of time.

2.3.4 Dynamic Light Scattering Measurement

Dynamic light scattering (DLS) is a great way to determine particle size quantitatively. A Malvern Zetasizer Nano ZS was used to perform measurements. Before measuring the sample, the cuvette was loaded with 200 nm polystyrene particle for calibration. Then we added sample solution to the cuvette and performed the measurement. The DLS software will display the particle population at different diameters after the measurement.

2.3.5 Fluorescence Microscopy

Fluorescence microscopy can be used for single-molecule fluorescence imaging. A custom-built inverted fluorescence microscope (Zeiss Axio Observer D1) was used for imaging. Three diode lasers at 405, 561, and 658 nm (Laserglow) were used as a light source. An oil-immersion 63× objective lens from Zeiss was used, and the collected emission light from the sample was imaged with an Andor iXon3 electron multiplying charge coupled device (EMCCD) camera. The

fluorescence microscopy can take a single image or record a time measurement with one laser or multiple lasers controlled by ImageJ.

2.4 Microfluidic Channel Assembly

A microfluidic channel was the platform used in this work to study vesicle fusion and aggregation. The experiment on the microscope is conducted with a multi-channel flow cell assembled with a piece of glass coverslip (Schott) and a quartz slide sealed with medical-grade acrylic adhesive sheets. The estimated channel volume is 20 μl. Inlet and outlet ports (LabSmith) were glued to the glass slides using epoxy. In experiments, Tygon microbore tubing was used to connect sample tubes and flow channels.

2.5 Surface Passivation

The piranha washed glass coverslips were passivated with a one-step method to coat BSA-biotin on the coverslip and prevent nonspecific interactions between the vesicles and the glass surface. Before the experiments, approximately 30 μL 5 μM BSA-biotin in TAEM and tween-20 solution was flown into the channel and incubated for 1 hour. Tween-20 were used to fix defects on the coverslip surface, and BSA-biotin was attached to the surface in order for biotin-streptavidin conjugation that immobilizes giant vesicles on the substrate. After the passivation processes, ~30 μL 1 μM streptavidin in TAEM buffer was added to the fluid channel. Without adding streptavidin, the GUVs with biotin moieties will not be attached to the surface.

3. LIPOSOME FUSION VIA DNA SIGNALS

3.1 Introduction

Liposomes are useful nanocontainers to encapsulate and protect both small and macro biomolecules, such as proteins and DNA. The engineering of liposomes has advanced to a level that enables the manipulation of their surfaces with specific ligands in order to improve their functionality. For example, proteins, carbohydrates, and vitamins have been used as targeting units to enhance the cellular specificity of these nanocontainers.[20] Moreover, some "smart" vesicle designs allow the release of the encapsulated cargo through physicochemical responses of the liposomal membrane to external stimuli or by incorporation of transport channels.[21] Membrane fusion, which has previously been shown for drug and gene delivery applications, is another technique liposomes can deliver their payload to cells.[22] In many cellular processes, including exocytosis, endocytosis, and the transfer of membrane proteins between cellular compartments, membrane fusion plays a crucial role.[23] Most membrane fusion events follow a similar order: docking, hemifusion, and full fusion.[10] As part of the docking process, membranes are brought into close proximity, which can cause the outer layers to merge, whereas the inner layers stay separated, resulting in hemifusion. Full fusion is achieved when the outside and inside layers of both membranes merge and content mixing occurs. Recently, several groups have reported hemifusion and full fusion of liposomes by exploiting Watson–Crick base pairing of complementary membrane-anchored oligonucleotides.[24,25] In these studies, DNA was grafted onto the liposomal surface using cholesterol or fatty acid derivatives conjugated at the 5'- or 3'-end of the DNA oligomers.[26]

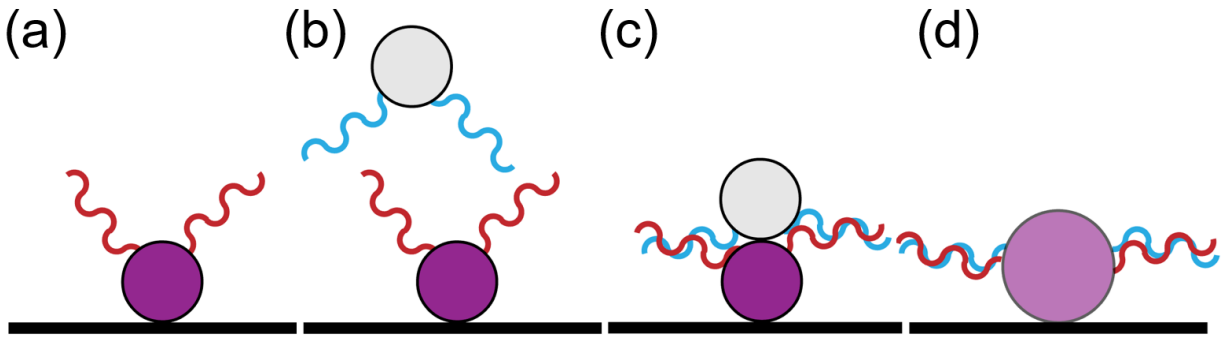

Figure 3.1. Schematic for liposome fusion induced by DNA signals (a) Small liposome encapsulated SRB and has linker strand on its surface is immobilized in glass surface with non-specific binding (b) Another type of small liposome with no SRB encapsulated and linker strand complimentary with the first one is introduced into the channel. (c) When two liposome collide, the complimentary DNA strands on adjacent liposome hybridized (d) The hybridization of membrane anchored DNA strand exert force to the adjacent membranes and induced liposome fusion.

3.2 Scheme

Figure 3.1 presents the scheme of our fusion experiment. Two types of DNA-decorated vesicles are prepared. The SUV that contains SRB is first introduced to the fluid channel, and immobilized on a glass surface with non-specific binding. The SUV contains cholesterol-DNA on its surface. Then, we flow in another type of SUV that does not encapsulate SRB. It contains a complimentary DNA strand to the first type of SUV. When the two SUV with complimentary DNA strand collides with each other, the DNA strands on their surface will be hybridized. The hybridization of the membrane-anchored DNA will exert force on the adjacent liposome membrane and force them to merge. When the fusion is completed, the SRB in the fused liposome is diluted, which will cause an increase in fluorescence intensity.

3.3 Experimental Methods

3.3.1 Materials

DNA sequence information

All the sequences were purchased from Integrated DNA Technologies and used without further purification.

Strand on SUV-A

CH5lp: /5Chol-TEG/TTACACGCCGCAGTTGACGGCCGTCCA

Strand on SUV-B

CH3lp: TGGACGGCCGTCAACTGCGGCGTGTAA /3Chol-TEG/

3.3.2 Sample Preparation Methods

Small vesicles with DNA strands

Small vesicles with complimentary DNA strands were prepared using a dehydration-rehydration method.[19] SUV-A contains CH5lp strand on its membrane, and encapsulated with 10mM sulforhodamine B (SRB). SUV-B contains CH3lp strand and DiD dye on its membrane. Cholesterol modified DNA and DiD dye (SUV-B only) were mixed with DPPC and DPPE at a molar ratio of 1:1:500:500 in a glass vial. The solution was dried in vacuum for 20 minutes to let lipids form a dry thin film on the bottom of the vial. Then, 1 mL PBS buffer with 10 mM SRB was added to the glass vial and the solution was placed on a pre-heat hot plate at ~90 °C. The solution was stirred with a stirring bar at 500 rpm for 1 hour while the temperature was kept all the time. After stirring, small vesicle solution was purified by centrifugation with a 30 kDa molecular weight cut off spin column at 5,000 g for 5 minutes. This process was repeated 6 times to remove unbound lipid and DNA molecules. From the molar ratio of components, we estimate roughly 50 oligonucleotides per small vesicle.

3.3.3 Characterization

DLS Measurement of SUV

To measure the performance of DNA signal induced lipid fusion, we measured individual small liposome samples as well as the SUV-A and SUV-B mixed solution with 1 to 1 ratio incubated at

20°C (room temperature), 37 °C, 50 °C for 1 hour. The DLS measurement shows that SUV-A, SUV-B, mixture at 20°C, mixture at 37°C, mixture at 50°C has an average hydrodynamic diameter of roughly 298, 313, 456, 604, and 636 nm, respectively, as shown in Figure 3.2. It is evident that with increased temperature, the percentage of fused liposomes increases, and therefore particles in the mixture solution have a larger average hydrodynamic diameter.

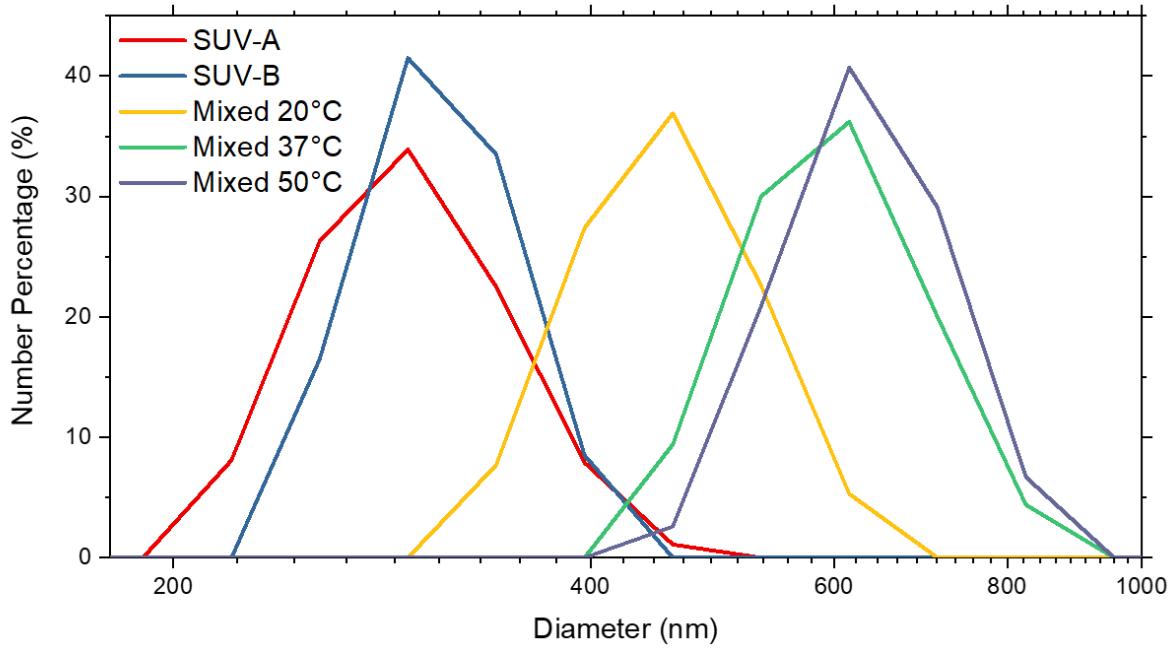

Figure 3.2. DLS measurement of SUV-A, SUV-B, and SUV-A and SUV-B mixed at 1 to 1 ratio at 20°C, 37°C, 50°C for 1 hour. The mixture at 20°C, 37°C, 50°C has an 49%, 98%, 108% increase in average hydrodynamic diameter respectively.

SRB self-quenching property

SRB was used as a fluorescent probe for studying vesicle fusion because of its self-quenching property below 20 mM. When a liposome encapsulated with SRB fuses with another liposome with no SRB, the fused liposome will have a stronger fluorescence intensity. SRB has its excitation and emission peaks at 566 and 583 nm, respectively. To determine the optimized SRB concentration for our experiment, we synthesized three sets of liposomes encapsulating 5, 10, and 15 mM SRB. The emission shows that the intensity is highest with 5 mM and decreases as the concentration increases (Figure 3.3). In our experiment, we used 10 mM SRB in SUV.

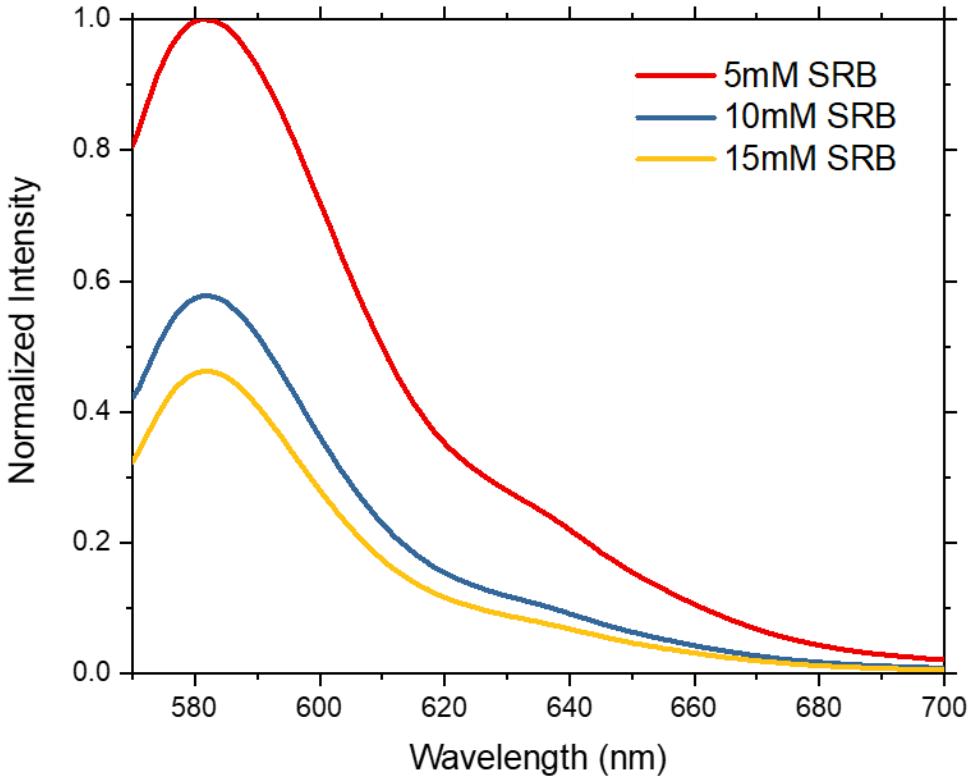

Figure 3.3. SUV encapsulated with different concentration of SRB. Fluorescence intensity changed more from 10mM to 5mM than from 15mM to 10mM. Therefore, we choose to encapsulate 10mM SRB in SUV.

3.3.4 Kinetic Measurement

To verify the fusion experiment, we measured the kinetics of fluorescence intensity of SUVs with uncomplimentary strands (CH5lp and 13w) and complimentary strands (CH5lp and CH3lp). Figure 3.4 shows that the fluorescence intensity increased by 30% with SUV-A and SUV-B, whereas the fluorescence intensity only increased by 5% with SUV-A and SUV-13w.

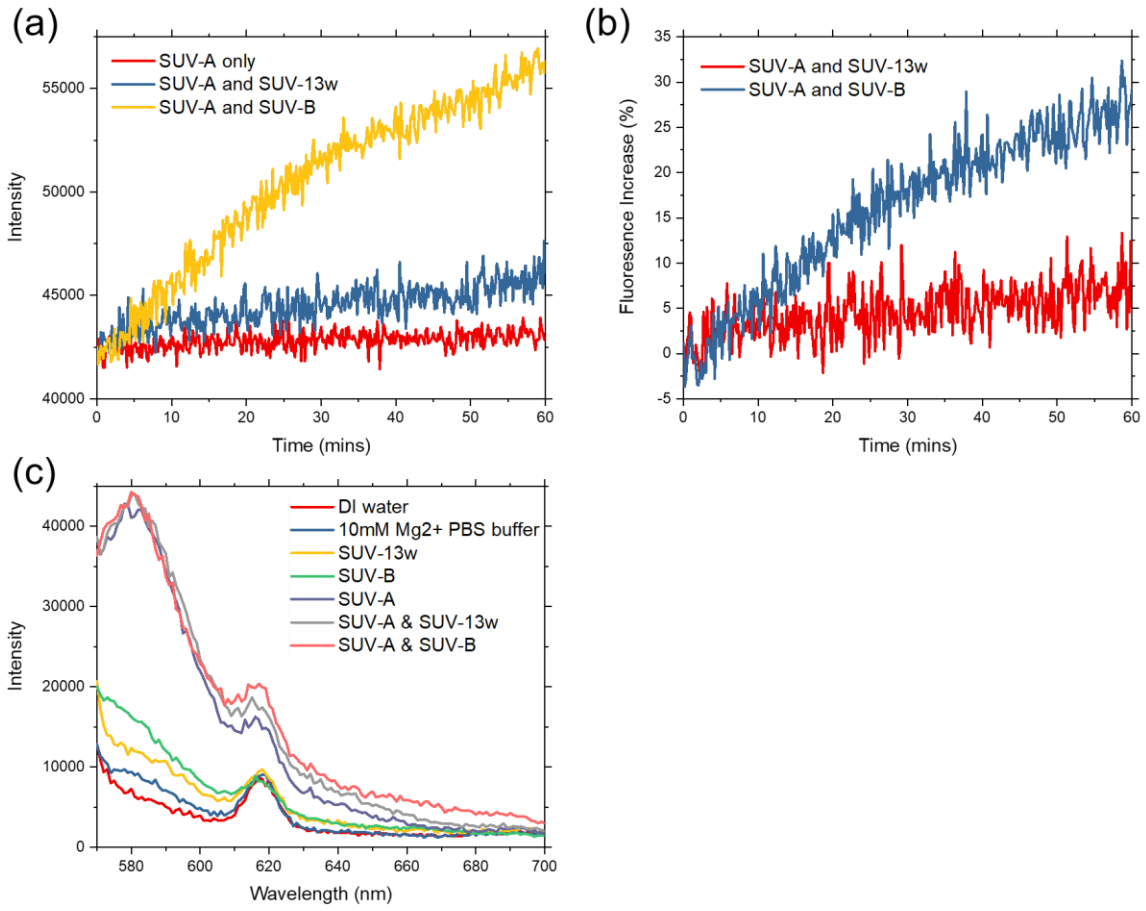

Figure 3.4. SUV kinetic fluorescence measurement. (a) Kinetic fluorescence measurement of SUV-A (encapsulated with SRB) only and SUV-A mixed with SUV-13w (uncomplimentary DNA strand) does not show significant increase of intensity at 582nm. Kinetic fluorescence measurement of SUV-A mixed with SUV-B shows 30% increase of fluorescence intensity in 1-hour period. (b) Fluorescence intensity increase with regard to SUV-A only (c) Control experiment, fluorescence intensity of DI water, 10mM Mg^{2+} PBS buffer, SUV-A, SUV-B, SUV-13w, SUV-A mixed with SUV-13w (at 0 min), SUV-A mixed with SUV-B (at 0 min).

3.4 Results and Discussion

For the fusion experiment, we studied two parameters that influence liposome binding, which are DNA and temperature. We first demonstrated DNA induced liposome fusion in the fluid channel. As discussed in Figure 3.1, SUV with SRB is first introduced into the channel and immobilized on the glass surface. After this step, we observed a stable fluorescence intensity indicating that SRB in the small liposome does not have significant leakage. Then, we flow in PBS buffer solution to remove all the SUV with SRB. Next, we flow in the SUV with complimentary strand to the first

type. This type of SUV does not encapsulate SRB, and has DiD dye on its surface, which is observed using 658 laser. Once the two types of SUVs collide with one another, both signals in 561 laser and 658 laser get large instantly. Then in the next few minutes, we observed a 40% increase in fluorescence intensity. This fluorescence increase is caused by the dilution of SRB probe, as shown in Figure 3.5a,b,c. This indicates that the two overlapped SUVs are fused. As a control experiment, we replaced the second types of SUV with an uncomplimentary strand. This time, when two type of small liposome collide in the fluid channel, there is no force to keep them adjacent to one another, and the small liposome with uncomplimentary strand touch and go. When we flow in SUV with uncomplimentary strand, we do not observe it overlapped with the SUV with SRB. The fluorescence intensity have no significant increase, as shown in Figure 3.5d. It shows that without the presence of complimentary DNA strand, no fusion will happen.

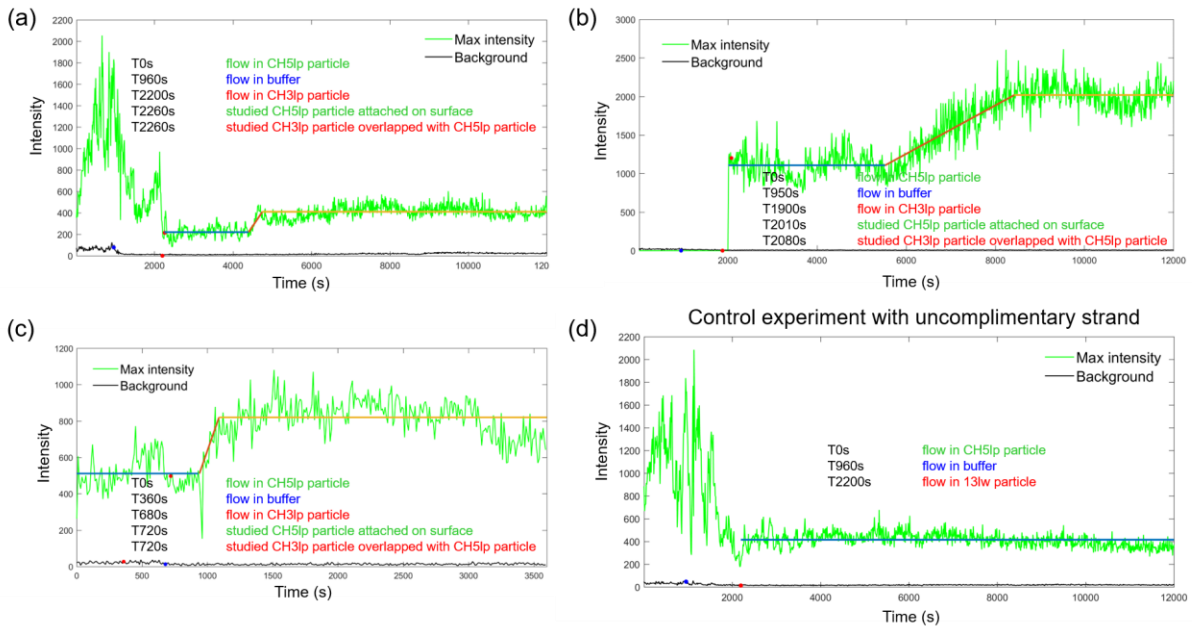

Figure 3.5. Single case study of lipid fusion in fluid channel at room temperature. (a,b,c)SUV with SRB was first flow into the fluid channel, and some of them are non-specifically bind on the coverslip. Then SUV with complimentary DNA strand is flow into the channel. Once the two types of SUV attached, the fluorescence intensity of SRB probe raise, indicating that the two overlapped SUV are fused. (d) SUV with uncomplimentary DNA strand does not overlap, and therefore we do not observe fluorescence increase.

Then, we studied the second parameter that influences liposome fusion, which is temperature. The general trend is that from room temperature (around 20 °C) to 50°C, with an increase in

temperature, more liposomes with complimentary DNA strands are fused. This is probably due to the increase of collision between the two types of small liposome, which is consistent with what we find in the DLS measurement, as shown in Figure 3.2. We visualized this difference by incubating SUV with complimentary and uncomplimentary DNA strand in an incubator at 20°C, 37°C, and 50°C for 1 hour. And they flow them into the fluid channel. Then we count the small liposomes that are immobilized on the glass surface and count how many liposomes with only one type of laser signal and how many liposomes with both types of laser signals to measure the overlap ratio. We observe that at all the temperature, liposomes with complimentary strand has a higher overlap ratio and the ratio increase with higher temperature. Here, each liposome's fluorescence intensity has large variation because the microscope is more focused in the center area, and is brighter in the center area. Therefore, it is hard to tell whether the overlapped liposome is fused or not by only comparing their fluorescence intensity. Still, the overlap ratio indicates that temperature has a significant influence on liposome fusion.

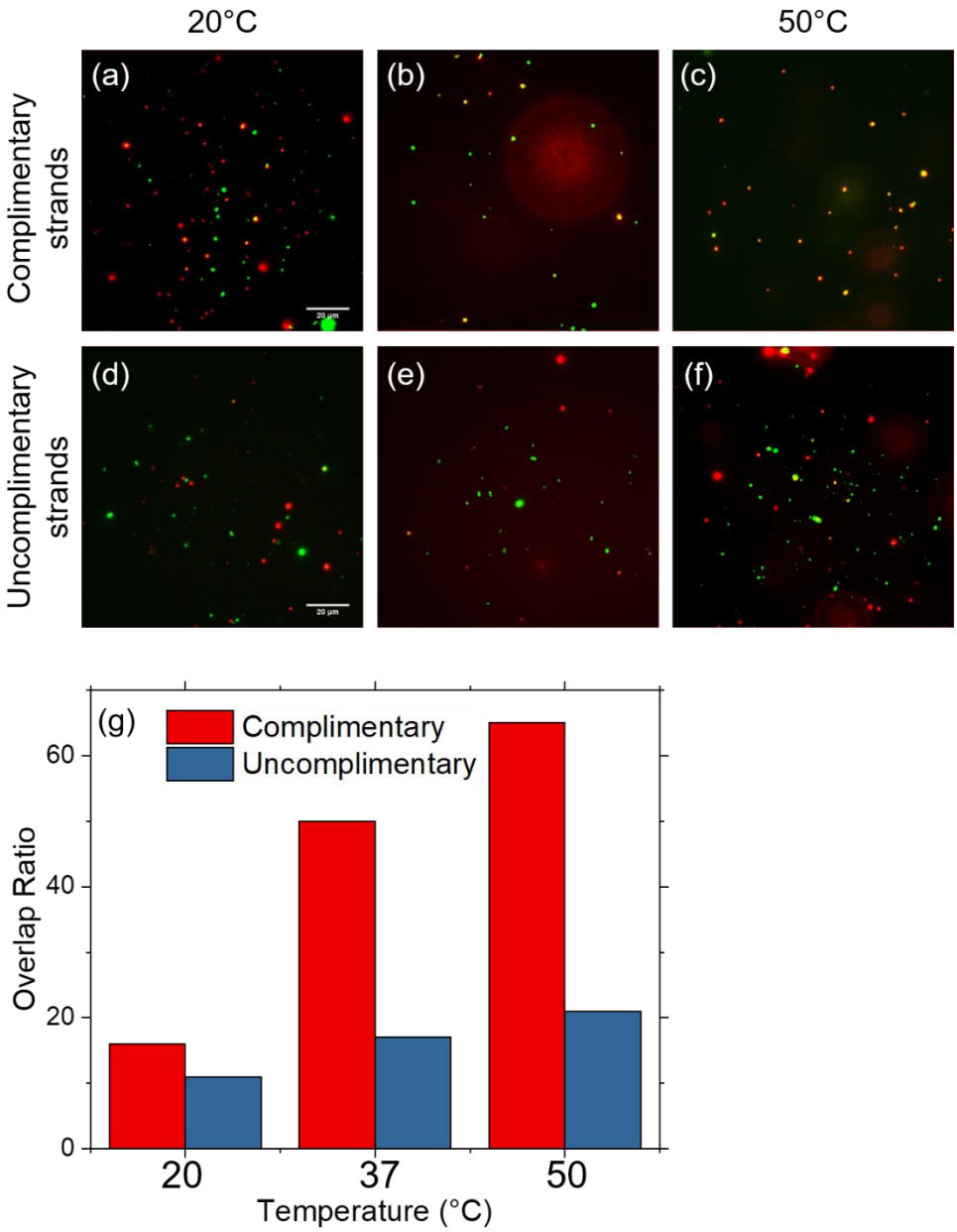

Figure 3.6. Temperature effect on liposome fusion. (a) 16% overlap of liposome with complimentary DNA strand incubate at 20°C for 1 hour. (b) 50% overlap of liposome with complimentary DNA strand incubate at 37°C for 1 hour.(c) 65% overlap of liposome with complimentary DNA strand incubate at 50°C for 1 hour. (d) 11% overlap of liposome with uncomplimentary DNA strand incubate at 20°C for 1 hour. (e) 17% overlap of liposome with uncomplimentary DNA strand incubate at 37°C for 1 hour. (f) 21% overlap of liposome with uncomplimentary DNA strand incubate at 50°C for 1 hour. (g) Overlap ratio in histogram

3.5 Conclusion

In this chapter, we have demonstrated vesicle fusion using DNA signals. The cholesterol modified DNA strands were adequate for this purpose. This study could help construct synthetic cells as a surrogate model system for cell biology research. For example, an artificial cell encapsulating drug or gene cargo could be delivered to a target cell and the payloads may be released. One application is the mRNA COVID-19 vaccine, which encapsulates the mRNA signal of the virus' spike protein in lipid nanoparticle. It is the first vaccine candidate launched into clinical trials. In summary, we envision that the growing library of DNA nanotechnology tools will open new opportunities for both fundamental sciences and novel biotechnology applications.

4. PROGRAMMABLE AGGREGAGATION OF ARTIFICIAL CELLS WITH DNA SIGNALS

4.1 Introduction

Cell aggregation is an essential phenomenon in biology, where cells cluster together upon external cues in a certain environment. Thus the study of intercellular signaling and cell-cell interactions during the process will greatly contribute to the understanding of cell differentiation, migration, and viability.[12-14] It also has great potential to improve research in tissue engineering as cell interactions are an important part of tissue construction.[27] Tissue engineering requires not only scaffold matrices that provide structural supports but also cellular signals to generate growth factors.[16] Major research efforts have been made on this subject, including signaling pathways and associated molecules, cell aggregation kinetics and dynamics, and related diseases, considering the importance of this topic.[28,29] However, with the sophistication of cellular environments, completely understanding the aggregation behaviors and effectively managing the processes is still a major challenge. A simplified synthetic system capable of communication and coordination between cells and cells will therefore help to gain a deeper understanding and precise control of cell interactions and behaviors.[30] Engineered lipid vesicles can serve as a flexible platform with cell-like structures and properties, resembling some biological cell characteristics.[6]

DNA nanotechnology has been explored to build and monitor synthetic cells over the past few years. DNA self-assembly with sub-nanometer precision can produce complex architectures,[31-33] dynamic nanostructures such as switches and motors,[34,35] and computing devices.[36] The main benefit is the outstanding programmability and structural predictability of DNA. DNA assemblies have been used for instance, to stabilize vesicle structures and control their shapes.[37,38] For programmable vesicle fusion, DNA base-pairing was introduced.[24,25] DNA origami has recently been used to imitate the form and function of membrane protein channels that occur naturally.[39-41] They have been integrated into lipid bilayer membranes and have acted as pores in and out of vesicles for biomolecular transport.[42] The kinetics of the transport process through DNA origami pores was measured with dye molecules.[43] With computer-aided molecular engineering tools that are available for DNA nanotechnology, the geometry and chemical functionality of this novel class of artificial nanopores can be rationally developed.[9,44-46] Protein or peptide membrane pores also

offer molecularly defined dimensions; however, their geometry cannot be changed as easily as for DNA nanostructures, and their chemical functionalization is usually more cumbersome.[47] These characteristics make DNA-based membrane channels highly promising biomolecular devices for single-molecule biosensing and drug delivery applications, or as artificial cell components.[48]

In this study, we demonstrate programmable communication and coordination between artificial cells by using transmembrane pores made of origami DNA. The engineered vesicles interact with each other and aggregate controllably and reversibly, as biological cells do. We establish new signaling pathways such that biochemical instructions for clustering behaviors are followed by the artificial cells. A series of external biomolecular signals are recognized and transported into the vesicles, where they are transduced to another form of signals that are transmitted through the origami membrane channels out of the cells, thereby initiating cell aggregation. To trigger vesicle aggregation and release, we use DNA oligonucleotides as single molecules, which are monitored by fluorescence microscopy. This device mimics biological cells' actions and offers valuable tools for study in cell biology and bottom-up synthetic biology.

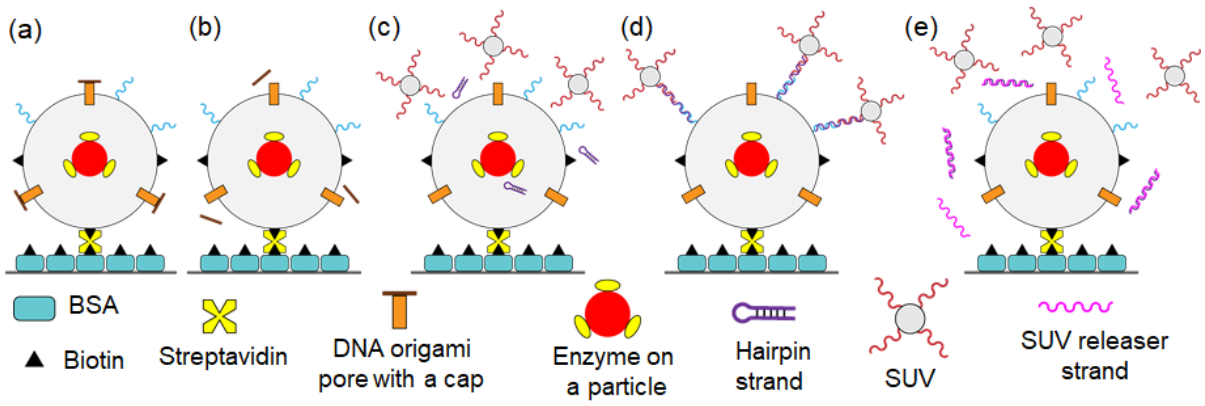

Figure 4.1. Scheme for reversible cell aggregation programmed by DNA signals. (a) By biotin-streptavidin conjugation, a giant vesicle is immobilized on a BSA modified glass surface. The GUV has DNA strands (shown in blue), has DNA origami tubule (orange) transmembrane channels, and encapsulates Exo III on a polystyrene particle (yellow-red). (b) The pores are initially closed with flat origami caps which can be removed by toehold-mediated strand displacement by 'cap-releaser' strands. (c) Via the membrane channels, an external DNA hairpin signal may reach the vesicle where it is transduced by Exo III into another type of signal through enzymatic reaction. The enzyme digests a portion of the hairpin from the 3 end, exposing the complementary domains on the vesicles for the strands (both blue and red). (d) Processed signaling oligonucleotides pass through the pores of the origami and cause several small vesicles to accumulate on the GUV. (e) By removing the linker strands, another DNA signal, 'SUV releaser' strands shown in pink, can dissociate the SUVs attached to the giant vesicle. It is possible to program this association and dissociation activity with DNA signals and continuously indefinitely in principle.

4.2 Scheme

Figure 4.1 presents the scheme of our experiment. Two types of DNA-decorated vesicles are prepared. The GUV includes origami tubular DNA pores built to have a diameter of ~32 nm and a length of ~60 nm (Figure 4.2). Each tubule is functionalized at half the length with cholesterol moieties to insert the origami during assembly into the GUV and stabilize it in the lipid membrane hydrophobic setting. By using two sets of staple extensions complementary to each other the DNA pores are initially covered with rectangular DNA origami caps. A set of staples has a 16-nucleotide (16-nt) extension on the tubular pore, while the rectangular cap comprises staples with a 24-nt extension (shown in pink and green in Figure 4.2, respectively). These staples are used to connect the 60-nm-100-nm rectangular tile to the rim of the DNA tubule. More than 90% of the tubular structures are linked with flat origami in the AFM images (Figure 4.3). Giant vesicles are immobilized via biotin-streptavidin conjugation on a glass coverslip (Figure 4.1a). With biotin

functionalized bovine serum albumin (BSA), the glass surface is passivated, and streptavidin is then added. Thus the GUV containing biotinylated phospholipids binds to the surface during the experiments and remains there.

Using a series of 'cap releaser' strands, the DNA pores, first closed with flat DNA origami caps, can be opened. An 8-nt single-stranded overhang at the 3' end has the staple extensions on the rectangular origami tile so that fully complementary cap releasers can remove them through toehold-mediated strand displacement,[49] as illustrated in Figure 4.1b. A hairpin, shown in purple, is used as a signal for cell-cell interactions. There are two domains of this strand; one is complementary to the giant vesicle strand (shown in blue), and the other can hybridize with the DNA on the small vesicles (red). These domains, however, are initially shielded within the hairpin structure, so they do not bind to the vesicle's DNA strands. The hairpin can reach the GUV through diffusion with the cap removed, where it can be opened by enzymatic cleavage (Figure 4.1c). Exo III enzymes are functionalized on a particle of polystyrene ~200 nm in diameter that is encapsulated in the giant vesicle. The split DNA signal can then spread out of the GUV and link the strands together on both giant and small vesicles, resulting in SUV aggregations on the GUV (Figure 4.1d). On the membrane of the small vesicles, rhodamine B is used, which is used for the imaging of SUV aggregation. Upon implementation of 'SUV releaser' strands through strand displacement, the small vesicles can disaggregate from the giant vesicle as the releaser strands are completely complementary to the SUV-linkers (Figure 4.1e).

4.3 Experimental Methods

4.3.1 Materials

DNA sequence information

Table 4.1. Sequences of DNA linker, releaser, and modified strands. The SUV linker can bind with both SUV and GUV strands, thereby connecting SUVs on a GUV. The hairpin strand includes the sequence of SUV linker which may be exposed after digestion of ACA TCT AAC AAC CAA ACC AT by Exo III. The GAA TCA part in the SUV linker is used as a toehold for the SUV releaser. In the cap releaser strand, AGT GCT GA is used as the toehold. Note that Cy5-DNA is a chimeric DNA/RNA oligonucleotide with rArU indicating RNA bases.

Name	Sequence
SUV strand	TAA CAA CCA AAC CAT TTT T /3CholTEG/
GUV strand	/amine/ GGA CAG AGT GAC ATC
SUV linker	ATG GTT TGG TTG TTA GAT GTC ACT CTG TCC GAA TCA
Hairpin signal containing SUV linker	ATG GTT TGG TTG TTA GAT GTC ACT CTG TCC GAA TCA ACA TCT AAC AAC CAA ACC AT
SUV releaser	TGA TTC GGA CAG AGT GAC ATC TAA CAA CCA AAC CAT
Cap releaser	TGT CAC TCT GTC CGA ATC AGC ACT
Cy5-DNA	/5Cy5/ GGT GGT GGT GGT TGT GGT GGT GGT GGG TCA CTC rArUG TCC GAA TCA GCA CTT TTT TTT TTT

Origami design

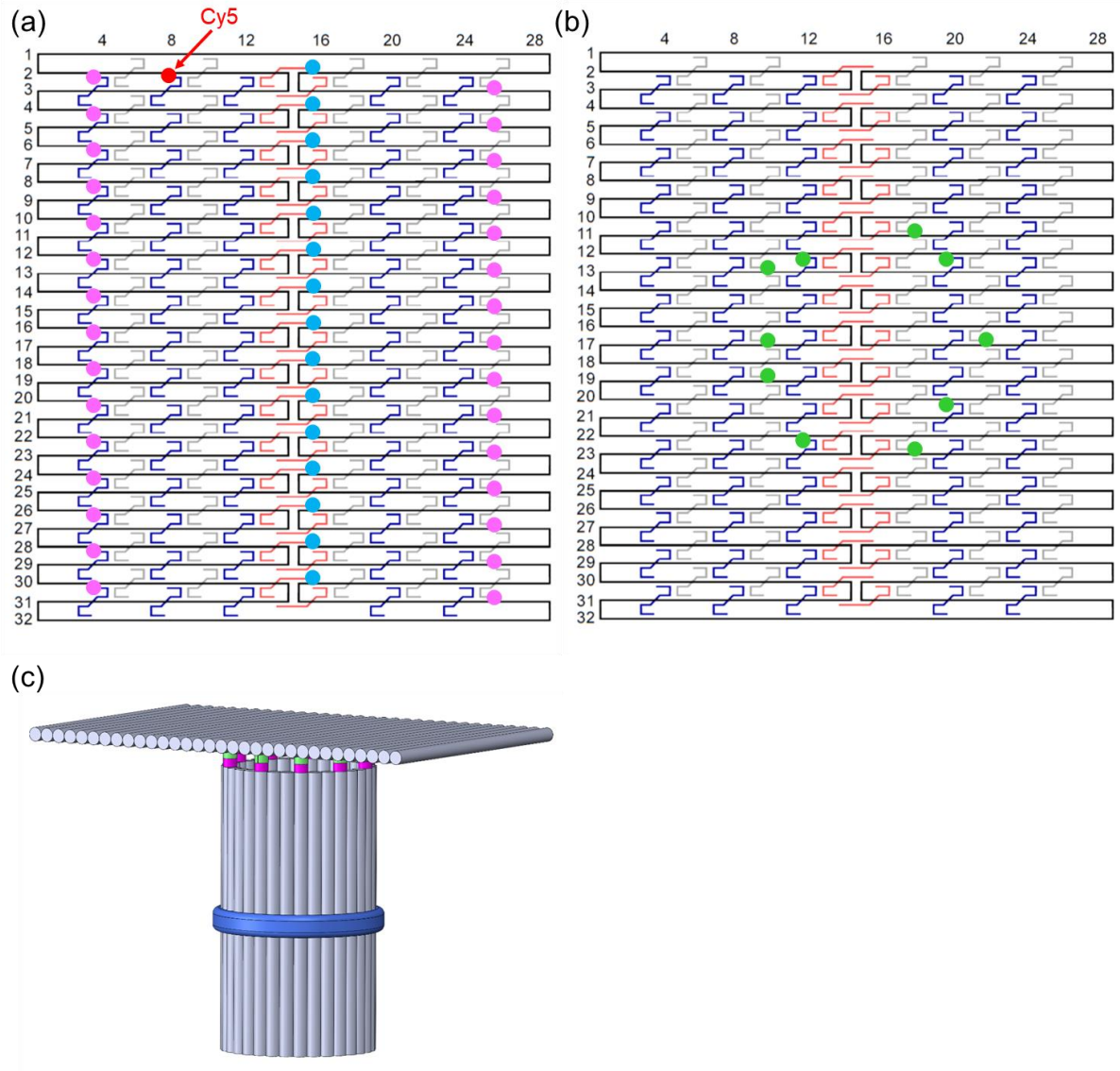

Figure 4.2. The origami designs and folding path diagrams for the tubular pore (a) and rectangular cap (b). (a) The 32-helix origami tile (identical in both (a) and (b)) before cyclization to form the tubular pore (see Table A.1 and A.2 for staples). A set of staples (termed tubular staples) are used to connect the top and bottom of the tile, forming a tubule (see Table A.3). The tubular staples are not shown in the schematic. A Cy5-DNA strand used for fluorescence imaging, shown in Figure 2a-b, is marked in red. A total of 30 staple strands (15 on each side) are added a 16-nt extension to connect the pore with the cap. The 15 staples marked in sky-blue are designed to link with cholesterol-DNA with a 27-nt extension (see Table A.2). (b) The rectangular origami cap. Each of 10 staples (indicated by green dots) have a 24-nt extension on 5' end: 16-nt (TTCGGACAGAGTGACA) for binding the pore, and 8-nt (AGTGCTGA) for toehold. (c) Schematic of the tubular pore closed with the rectangular cap. The sky-blue stripe represents the cholesterol moieties. The pink and green denote the staple extensions for capping.

4.3.2 Sample Preparation Methods

Conjugation of DNA to lipid molecules

DNA-lipid conjugates are used as components of DNA-decorated GUVs. The method for conjugation is as described in a previous report.[30] The method is a two-step process. The first step is a modification of DNA with azide group. The amine modified DNA strands in Table 4.2 were synthesized with azide-N-hydroxysuccinimide or azide-NHS in dimethylformamide or DMF, and triethylamine (TEA) was added as catalyst. The mixture was incubated at room temperature in shades for two hours to achieve complete reaction. Then, we added 200 µL ethanol and 10 µL 4 mM NaCl into the solution and froze it at -20 °C for 30 minutes to precipitate DNA. The solution was then centrifuged at 20,000 g for 30 minutes. The precipitate was re-dispersed in 200 µL ethanol and centrifuged for several times to remove excess azide-NHS molecules. After centrifugation, the precipitate was dried in vacuum and re-suspended in 1x PBS. The concentration of synthesized DNA-azide was determined by the absorption of the sample at 260 nm using a Perkin-Elmer Lambda 950 UV/visible/NIR spectrophotometer.

The second step is a conjugation of azide-DNA with DSPE-PEG(2000)-DBCO. DBCO can react with azide by click chemistry. DNA-azide from the last step was mixed with DSPE-PEG(2000)-DBCO at a molar ratio of 1:5. The mixture was then purified with centrifugation and ready for use.

Polystyrene particles with Exo III

Approximately 5 µL 10 µM Exo III enzyme (New England Biolabs) was mixed with 2% polystyrene particle solution (Thermo Fisher Scientific) diluted in 70 µL 2-(N-morpholino) ethanesulfonic acid (MES) buffer (pH 6.0). Then, 5 µL 100 µM 1-ethyl-3-(3-dimethylaminopropyl)carbodiimide (EDC) was added to the mixture as catalyst. In order to keep the activity of Exo III molecules, the mixture was kept at 4 °C for 3 hours. After the reaction was completed, the mixture was purified with the centrifugation method to remove the excess enzymes. The extinction coefficient of polystyrene particle is approximately $2x10^9$ $M^{-1}cm^{-1}$ at 660nm. It is measured that the polystyrene concentration is 0.19nM. Exo III is estimated around 1nM. Therefore, an average of 5 Exo III enzyme attached per polystyrene particle.

The enzymatic activity of Exo III after conjugation with polystyrene particles was examined by measuring the change of the fluorescence peak intensity from a DNA duplex modified with fluorescent dyes. One strand was conjugated with FAM dye (5' – ATC GGT CAG GCT T/iFluorT/T TTTTTT T – 3') and the other has a quencher on its 5' end (5' – /5IABkFQ/ AAG CCT GAC CGA T – 3'). When the two strands are hybridized, the quencher can absorb the fluorescence from the FAM dye, thus no fluorescence will be observed. If the duplex is digested partly by the enzyme, strong fluorescence will emerge. To test the Exo III activity, 1 μM of each DNA strand was dissolved in 100 μL 1x NEB Buffer (B7001S, New England Biolabs) first and measured fluorescence. Then, the measurement was paused, 1 μL conjugated Exo III particle solution was added into the solution, and the measurement was resumed. From the change of FAM fluorescence, the activity of Exo III was evaluated.

Assembly of DNA origami structures

As described in Figure 4.2, two DNA origami structures were used in this study. A tubular origami was designed as a transmembrane pore, while the rectangular tile was used for capping the pore. The design of the DNA tubule is identical with that of the origami rectangle except for the use of tubular staples.[50]

The origami tubules were prepared by mixing 10 nM scaffold strands, 4× DNA staples (Tables A.1 and A.2), 14× tubular staples (Table A.3), and 160× cholesterol modified DNA in 1× TAEM buffer (an aqueous solution of 40 mM trisaminomethane, 1 mM ethylenediaminetetraacetic acid (EDTA) disodium salt, 20 mM acetic acid, and 10 mM $MgCl_2$ at pH ~8). Note that cholesterol DNA is used for the insertion into lipid membranes. The mixture was then annealed in a Bio-Rad S1000 thermal cycler from 75 °C to 4 °C at -1 °C per minute.

The origami tiles were synthesized by mixing 10 nM scaffold strands with 4× DNA staples (Tables A.1 and A.2) in 1× TAEM buffer. The annealing of the mixture went from 75 °C to 4 °C at -1 °C per minute in the thermal cycler.

The origami tubules and tiles were purified 3 times by using the centrifugal filter (100 kDa) from Amicon. Then, the purified tubules and tiles were mixed at 1:2 molar ratio for assembly of capped

origami pores. After that, the mixture was annealed from 55 °C to 4 °C at -1 °C per minute in the thermal cycler.

4.3.3 Characterization

AFM images of tubular and rectangular DNA origami

We conjugated origami tiles with DNA tubules with a molar ratio of 2:1 to ensure as many origami pores capped as possible. We performed AFM imaging to examine whether the origami tubules are closed with flat origami caps as designed in Figure 4.2. For deposition of samples for AFM imaging, the target sample was diluted to 1.0 nM with TAEM buffer. Then, an aliquot of 10 μL diluted sample was pipetted onto the mica surface for 5-minute incubation at room temperature. After that, the mica was blown dry with compressed air, rinsed with 80 μL deionized (DI) water for about 3 seconds, and then blown dry again with compressed air.

AFM imaging was performed in the air using the Peak-Force tapping mode with a Bruker Dimension Icon AFM and SCANASYST-AIR probes. The images show that more than 90% of the examined tubules are connected with flat rectangular tiles (Figure 4.3). The connection is also confirmed by the height profiles. After the cap releasers were incubated for 1 hour, nearly 90% of the tubules are detached from the flat origami, confirming that the cap releasers are effective in removing the caps and opening the origami pores.

Figure 4.3. AFM images of DNA origami. (a) Near 100% flat origami rectangles, which measure approximately 60 nm x 100 nm in dimension. (b) The majority of DNA origami measures approximately 60 nm x 50 nm with a thickness of ~4 nm, which is roughly half the size and twice the thickness of the origami rectangle. The results indicate the identity of the tubular structure of the origami in solution, which should have a diameter of ~32 nm and a length of ~60 nm. Note that the tubular structures collapsed into a rectangular shape to maximize their contact with the mica substrate. (c) Origami structures after connecting tubules with tiles at a ratio of 1: 2. Most tubules are connected to flat tiles, while the linked origami structures in 3D collapsed before or during the AFM imaging. (d) Zoom-in of the black square area in (c). The scale bar is 20 nm. Colored lines (blue, red, and pink) denote the sites where heights are measured. (e) Corresponding height profiles of the objects in (d). Cross-sections of a flat tile (blue), an isolated tubule (red), and a tubule connected with a flat tile (pink). Dashed line indicates the mica substrate. The profiles confirm the connection between the tubule and flat tile. (f) Origami tiles and tubules after mixing with cap releaser strands. The majority (~90%) of the tubules are separate from the tiles, suggesting that cap releasers are effective in removing the flat caps from the tubules.

Figure 4.3 continued

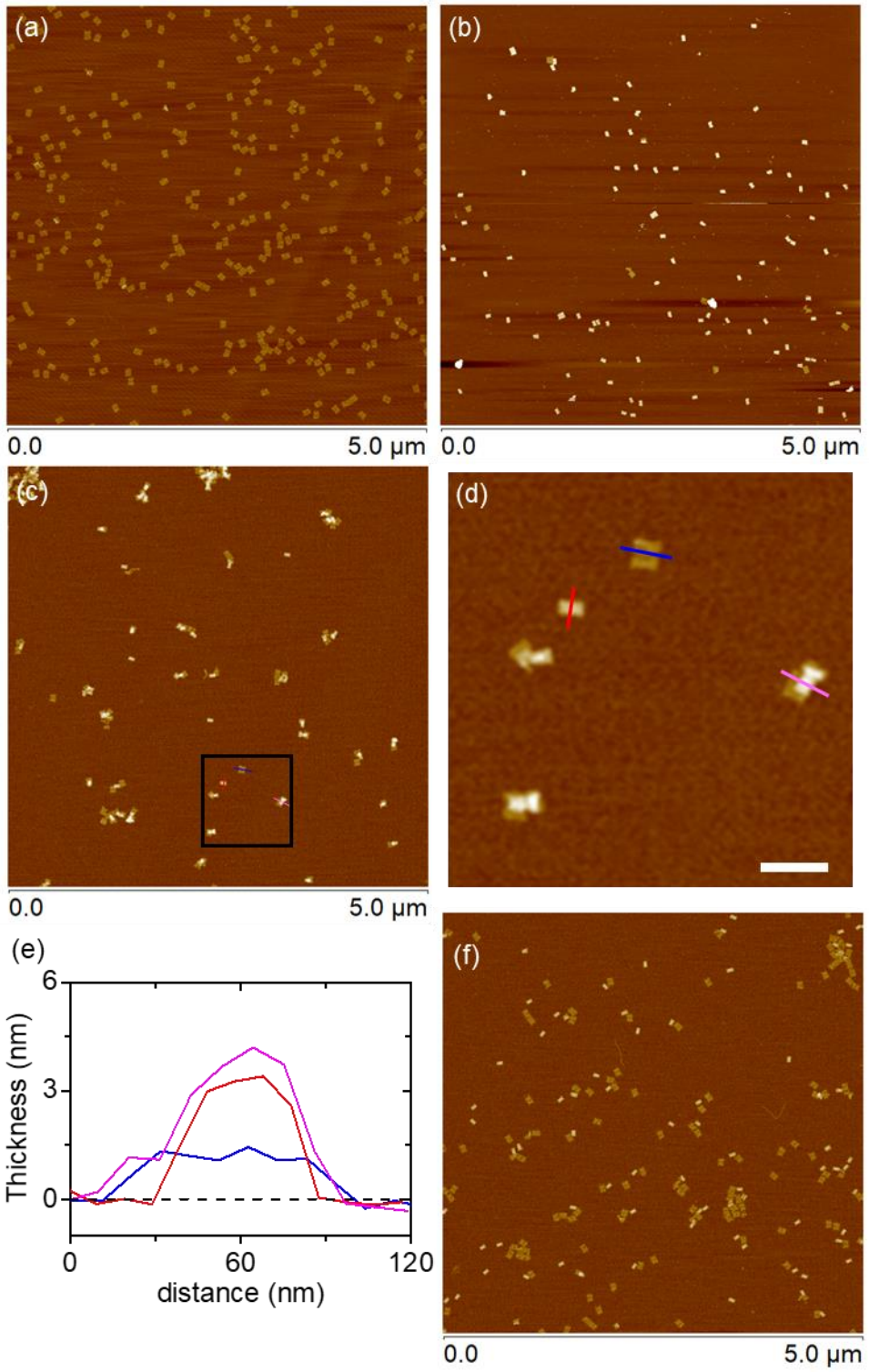

Exo III activity inside a giant vesicle

In our experiment, Exo III enzymes are used to transduce external DNA signals to another form of signals inside a giant vesicle. For example, the hairpin strand was partly digested by the enzyme, which exposes the SUV linker domain. The enzymes are functionalized on the surface of polystyrene particles with a diameter of ~200 nm. With the particle, the enzymes will not pass through the origami channels that have a diameter of about 32 nm. To prove that Exo III is functional inside the giant vesicle, we examined Exo III activity with both enzymes in free solution and particle-enzymes inside a GUV using a fluorophore-quencher pair. We used a FAM modified strand (termed FAM-DNA) and its complementary strand with a quencher group (quencher-cDNA), as discussed above. When hybridized, the quencher will absorb the emitted fluorescence from the FAM-DNA. For testing the free Exo III enzymes, we first prepared a 1 μM FAM-DNA solution which has a high fluorescence intensity. Then, we added the solution of cDNA-quencher at a ratio of 1:1, and the fluorescence intensity immediately dropped. Next, we added 1 nM Exo III that will digest the cDNA-quencher. The fluorescence intensity increased (Figure 4.4a), indicating that Exo III cleaved off cDNA and FAM-DNA is thus released.

We also examined the activity of the particle-modified Exo III enzymes and repeated the previous experiment. Again, we observed a sharp increase of the fluorescence intensity after adding enzyme-particles to the FAM-DNA/cDNA-quencher solution, as shown in Figure 4.4b. Next, we encapsulated the particle-Exo III into the giant vesicles with open origami pores. This time, the fluorescence intensity increase was small, yet distinct upon the addition of GUVs containing enzyme-particles (Figure 4.4c and 4.4d). We note that the degree of fluorescence recovery upon addition of Exo III varies significantly. For example, the fluorescence recovery with particle-modified enzymes is much less than that with free enzymes, and it is even smaller with particle-enzymes inside giant vesicles. This may be attributed to the fact that the number of enzymes was reduced significantly during the processes of conjugation, assembly, encapsulation, and purification. Further, the diffusion of oligonucleotides into and out of vesicles through origami channels may present another barrier. Nonetheless, our experiment clearly demonstrates that DNA signals can be received, transduced, and transmitted by synthetic cells, which is used to program reversible aggregation behaviors.

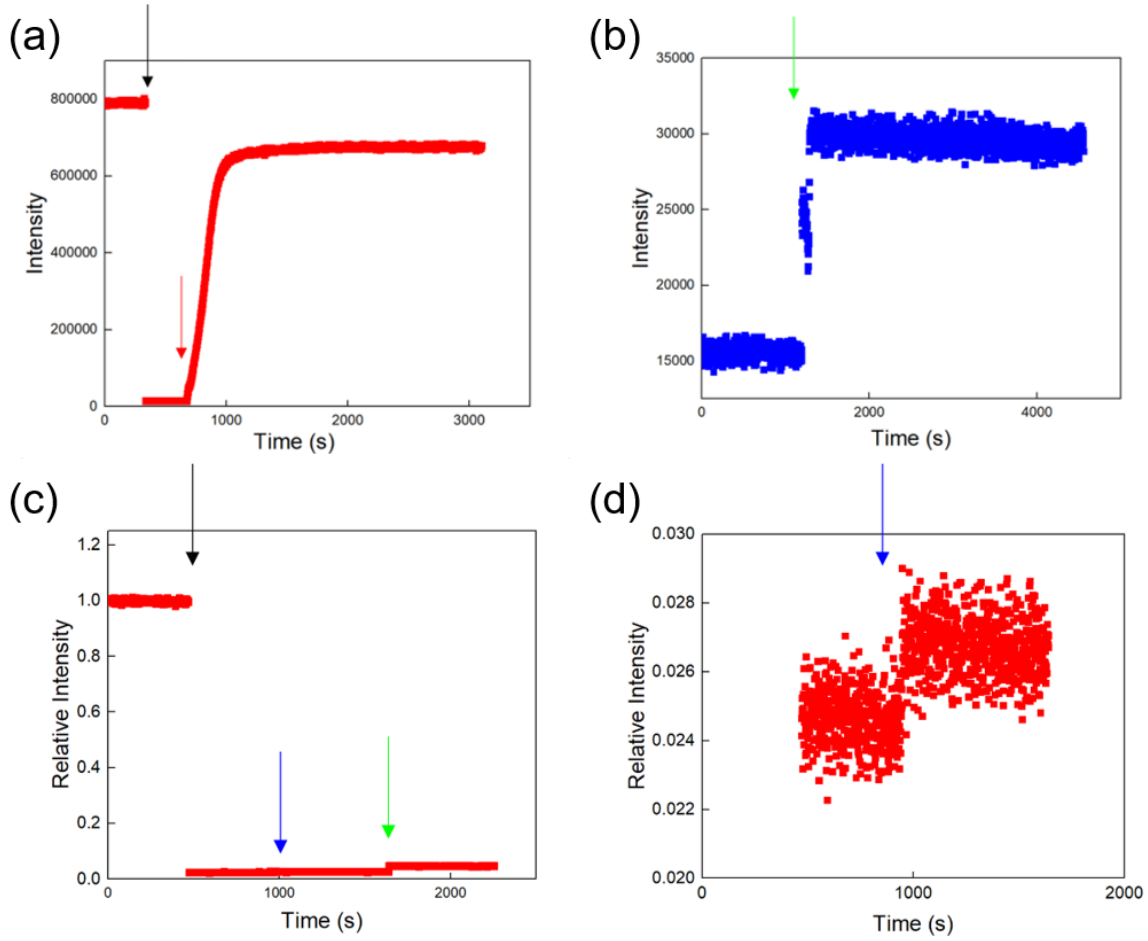

Figure 4.4. Exo III activity measured with a FAM-quencher pair in solution. (a) Fluorescence measurement with free Exo III enzymes. Initially, fluorescence is measured from 1 μM of FAM-DNA in solution. Upon addition of quencher-cDNA at 1 μM (black arrow), the fluorescence intensity immediately drops. After a few minutes, we added 1 nM Exo III enzymes into the solution (red arrow), which results in the increase of fluorescence intensity. (b) Fluorescence measurement in a similar experiment with particle-Exo III rather than free enzymes. The addition of polystyrene particle modified Exo III enzymes into the solution of FAM-DNA and cDNA-quencher (1 μM each; green arrow) leads to the increase of fluorescence intensity. (c)-(d) Fluorescence measurement with enzyme-particles encapsulated in giant vesicles with open origami pores. Black Arrow indicate the addition of cDNA-quencher into the solution of FAM-DNA (1 μM each). Then, GUVs containing enzyme-particles are added to the solution (blue arrow). A small, yet distinct increase of the fluorescence intensity is observed. After a few minutes, particle-Exo III (without vesicles) are added directly to the solution (green arrow), which results in a further increase of the fluorescence intensity.

As Exo III can digest DNA in a duplex from the 3' end, it is important to measure how it will interact with origami channels. We incubated the particle-modified Exo III with DNA origami tiles for 15 mins, and then performed the AFM imaging. Note that 15-min incubation was used because

it takes about 15 mins to encapsulate particle-Exo III in the giant vesicles with DNA origami channels. Figure 4.5 shows that most of the origami rectangles maintain their original shape. The results strongly suggest that the Exo III will not damage origami structures significantly under the experimental conditions.

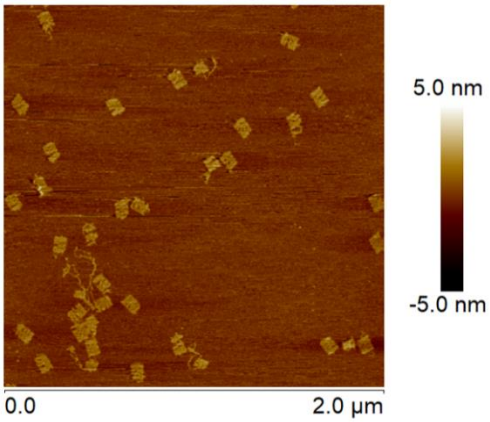

Figure 4.5. AFM image of DNA origami tiles after incubation with Exo III. Approximately 10 nM DNA origami tiles were mixed with 0.1 nM Exo III enzymes in 10 µL TAEM buffer for 15 mins. The AFM image shows that most of the rectangular origami remains its original shape, indicating that this concentration of Exo III will do little damage to the origami.

Immobilized GUV shape change over time

During the microscope observation, we find that several the vesicles that change the shapes and sizes over time. Our observation suggests that the immobilized vesicles gradually flatten over time as additional binding occurs between the vesicles and the surface. Further, we also noted that the flow in the imaging chamber may cause some change in the vesicle shape as shown below in Figure 4.6.

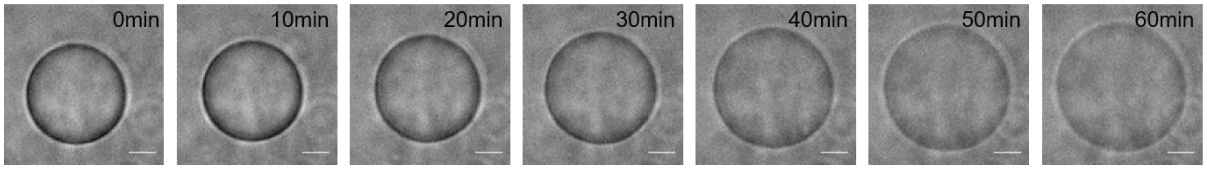

Figure 4.6. Shape change of a GUV during a one-hour period. Scale bar: 5 µm.

4.3.4 Kinetics

In Figure 4.8, we used a single exponential function $I(t) = ae^{k_f t} + b$ for curve-fitting of fluorescence intensity *I(t)* as a function of time *t*, which is related to outflux of GFP and Cy5-DNA molecules from giant vesicles. Here, k_f is the leaking rate, and *b* represents the energy barrier that inhibits further translocation of fluorescent molecules via DNA channels. The outflux kinetics of GFP and Cy5-DNA are expressed as:

$$I_{GFP}(t) = 0.8907e^{-0.3358t} + 0.3692$$

$$I_{DNA\ Dye}(t) = 0.6402e^{-0.1302t} + 0.3321$$

The kinetics of dFITC influx into a vesicle via origami pores in a previous report by Thomsen et al.[43] is expressed as:

$$I_{dFITC}(t) = 0.8106e^{-0.06495t} + 0.1834$$

Thus, the three leaking rates are similar within the order of magnitude ($k_{f,GFP} > k_{f,Cy5\text{-}DNA} > k_{f,dFITC}$) and the time constants are about 3, 8, and 15 mins for GFP, Cy5-DNA, and dFITC, respectively.

4.4 Results and Discussion

Figure 4.7 confirms the giant vesicles with DNA origami pores. The synthesized GUVs have a range of diameters from 5 to 25 μm. For optical imaging, we labeled the origami tubules here with Cy5 dye. On the microfluidic tube's bottom surface, the giant vesicles were immobilized and the imaging was carried out using a 63x objective lens under an inverted microscope. A separate ring in pseudo-red color is seen around the vesicle in the fluorescence image compared to the bright field image (Figure 4.7a), confirming the presence of DNA origami pores. In comparison, when cholesterol was not used in origami DNA, no fluorescence from the GUV was observed (Figure 4.7b). This means that as expected, DNA tubules are not incorporated in the lipid bilayer. We then tested molecular diffusion on the GUV containing origami tubules through open transmembrane channels (without caps). Green fluorescent protein (GFP) and 60-nt DNA labeled Cy5 were used in the calculation here. The fluorescent molecules were delivered to the giant vesicles in a 12.5 mM MgCl22 buffer containing tris-acetate-ethylene diaminetetraacetic acid (EDTA) (termed TAEM buffer). As shown in Figures 4.7c and 4.7e, the fluorescence intensity within the GUVs increased shortly after the inflow. However, fluorophores do not penetrate the vesicles without origami pores, so no fluorescence has been found (Figure 4.7d and 4.7f).

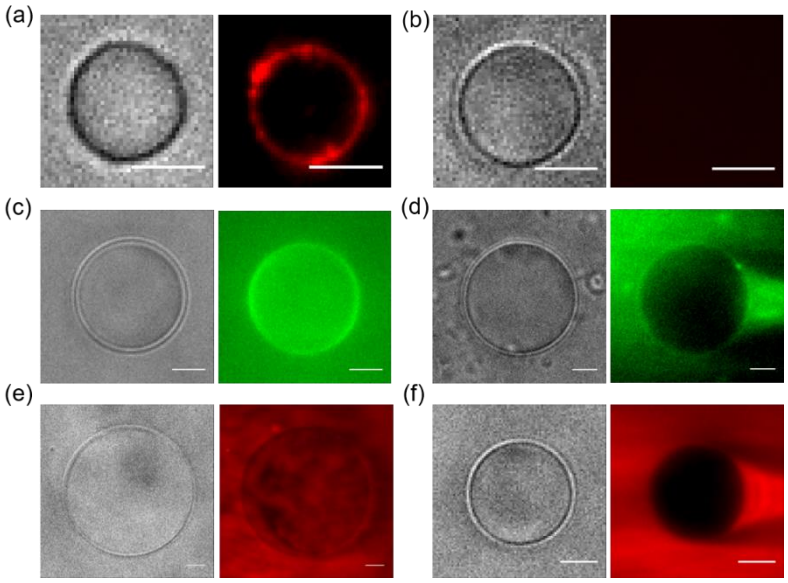

Figure 4.7. Brightfield (left) and fluorescence (right) images of giant vesicles. GFP is shown in a green color in fluorescence images and Cy5 is shown in red. (a) DNA tubules modified by cholesterol may be integrated into the vesicle membrane. A distinct, ring-shaped fluorescence pattern around the vesicle boundary is shown by the Cy5 functionalized origami. (b) Origami DNA cannot be injected into the membrane without cholesterol moieties, so no fluorescence is observed. (c) via transmembrane channels made of tubular origami, GFP can penetrate into the vesicle. (d) GFP cannot disperse into the vesicle without DNA tubules. (e) With DNA pores, Cy5-DNA may join the vesicle. (f) When no origami pores are present on the surface of the vesicle, the fluorophore-labeled DNA cannot pass into the GUV. Notice that with Cy5 dyes, the origami tubules in (c and e) are not functionalized. Scale bars are 5 μm.

To characterize the outflux through the membrane channels, we measured the kinetics of GFP and Cy5-DNA from the giant vesicles (Figure 4.8). The fluorescent molecules were initially encapsulated inside the GUVs containing the DNA pores with the flat origami caps on. Initially, the fluorescence intensity does not change, showing that there is no substantial leakage of dye molecules closing the origami pores. A dramatic decrease in fluorescence intensity within the vesicle was observed within a few minutes when the cap releasers were supplied to the channel (indicated by the orange arrows in Figure 4.8b,d). The fluorescence decreased until about 40 percent of the initial intensity was reached. We superimposed the fluorescence images (shown in pink) at the beginning and end of the measurements with the bright field images to display the dramatic changes (Figure 4.8a,c). It should be noted that GFP and Cy5-DNA outflows are identical and that after a long period of time, a fraction of fluorescent molecules remains within the vesicle.

The decrease in fluorescence was curve-fitted with a single-exponential function, giving a time constant of ~3 min for GFP and ~8 min for Cy5-DNA. These timescales agree well with the previously reported value (~15 min) using 40 kDa dextran with fluorescent moiety by Thomsen *et al.*[43]

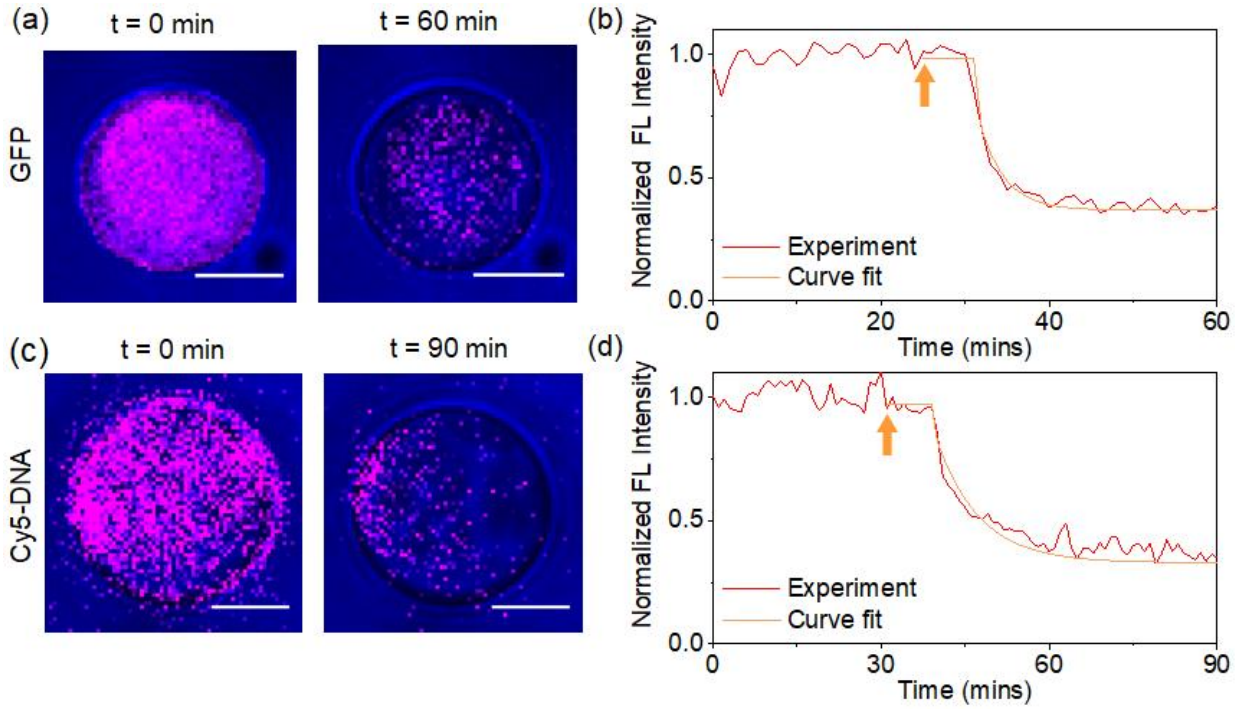

Figure 4.8. Kinetic measurement of molecular outflux through origami pores from giant vesicles immobilized on the glass coverslip surface. (a) Fluorescence images of GFP molecules (shown in pink color) overlaid with brightfield images of a vesicle at time t = 0 and 60 min. The molecules, initially encapsulated in the GUV, diffuse out of the vesicle after the pores are opened. (b) The fluorescence intensity inside the vesicle decreases, shortly after the cap-releaser strands were introduced into the microfluidic imaging chamber (indicated by the orange arrow). The exponential curve-fit (orange line) suggests a time constant of ~3 min. (c) Fluorescence images of Cy5-DNA inside a giant vesicle overlaid with brightfield images at time t = 0 and 90 min. (d) The fluorescence diminishes after adding the cap releasers (orange arrow) with a ~8-min time constant. Scale bars are 5 µm.

Additional kinetic measurement

To measure the kinetics of molecular transport via origami channel, we used GFP and Cy5-DNA in the outflow experiment (Figure 4.8 and Figure 4.9). GFP and Cy5-DNA were initially encapsulated inside the giant vesicles at a concentration of ~2 µM. The origami channels were initially closed with the flat origami tiles. The fluorescence intensity did not change without adding

cap releaser strands to open the origami pores, indicating no significant leak of fluorescent molecules from the GUV. After ~25 mins of the observation, we added the cap releasers as indicated by black arrows in Figure 4.9b and 4.9f. Shortly after that (roughly 5 mins), the fluorescence intensity inside the GUV started to drop. The intensity continued to decrease over time. However, the intensity inside the GUV was still higher than the background after 90 mins. In the control experiments (Figure 4.9c,d,g,h), the giant vesicles contained the fluorescent molecules but did not include origami pores. As expected, no significant changes in the fluorescence intensity were observed, indicating that there will be no molecular diffusion in and out of the vesicle without origami channels.

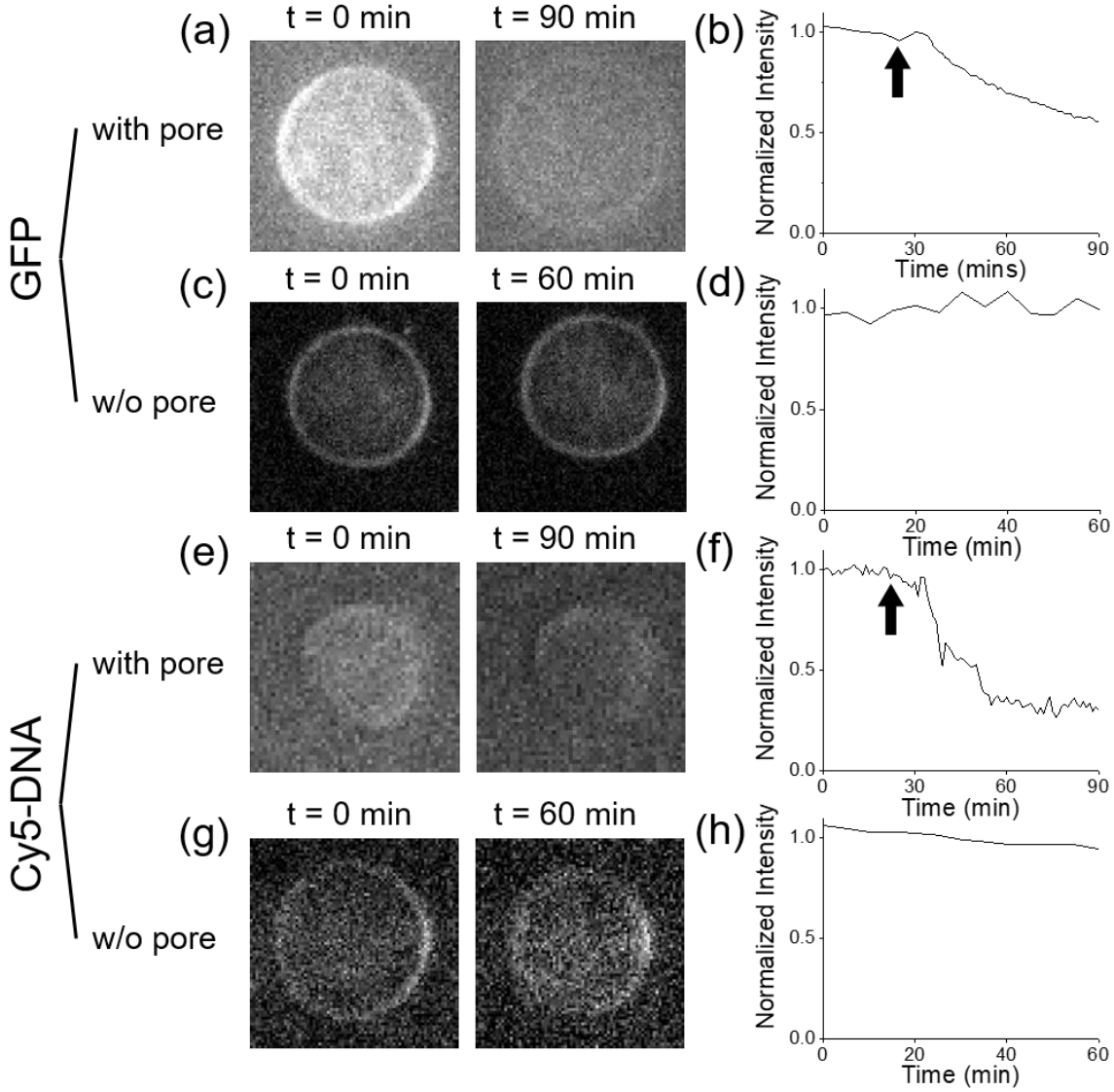

Figure 4.9. Kinetic measurements of molecular transport through DNA origami pores. (a) Fluorescence images of GFP molecules initially encapsulated inside a GUV at the beginning (t = 0 min) and end (t = 90 min) of the experiment. (b) Normalized fluorescence intensity of GFP as a function of time. After 25 mins, the cap releaser strands were introduced to the imaging chamber to remove the origami caps and open the channels, as indicated by the black arrow. Shortly after that, the fluorescent molecules diffused out of the GUV, and the fluorescence intensity inside GUV dropped. (c)-(d) Control experiment with the GUV containing GFP, but without origami pores. The fluorescence intensity does not change significantly, indicating that no molecular transport in and out of the vesicle without pores. (e)-(f) Fluorescence measurement of Cy5-DNA encapsulated inside a giant vesicle over time. Fluorescence images at the beginning and end of the experiment (t = 0 and 90 min, respectively). Shortly after adding cap releaser strands (black arrow), the fluorescence intensity inside the GUV dropped. (g)-(h) Control experiment with the GUV encapsulating Cy5-DNA without origami channels. The fluorescence intensity remains constant over time without origami pores.

Reversible aggregation behavior using DNA signals

We examined the DNA-programmed reversible clustering of vesicles. To test the effectiveness of the SUV linkers and releasers, the origami pores and the Exo-III modified particles were not included in the large vesicle, while the SUVs and GUV have unique strands shown in red and blue in Figure 4.1. On the imaging surface, we first immobilized a large vesicle (state I Figure 4.10a). Then, 36-nt SUV linkers were supplied to the microfluidic channel along with SUVs with complementary domains to the strands on the small and large vesicles (indicated by the red arrow). For the SUVs and 10 nM for the SUV linkers, the final concentrations were around 1011/ml. The TAEM buffer was given after 10 minutes of incubation to wash away unbound small vesicles and excess linker strands. Around the broad vesicle boundary (state (ii)), distinct fluorescence is observed, suggesting that the small vesicles actually accumulate as planned on the GUV surface. Note that since the giant vesicle does not contain any fluorophores, the fluorescence intensity originates from the SUVs. We then provided the SUV releaser strands, indicated by the black arrow, to the imaging chamber. The invading strands first communicate through 6-nt toehold with the SUV connectors and completely attach with them, removing the connectors from both the small and large vesicles. As a consequence, the SUVs dissociate from the GUV and, as seen in the state, the fluorescence intensity drops (iii). By attaching the connectors and releasers in sequence, the aggregation and disaggregation of the tiny vesicles on the GUV has been repeated. As shown in Figure 4.10a, the fluorescence intensity varies accordingly. Such a reversible aggregation can in principle, be indefinitely cycled. In a control experiment, we replaced the SUV linkers with random sequence strands (indicated in Figure 4.10b by the blue arrows) that should not be base-paired with the vesicle strands. Indeed, vesicle aggregation was not caused and, as shown in Figure 4.10b, no major changes were observed in the fluorescence intensity. This confirms that only engineered DNA signals can contribute to the action of aggregation.

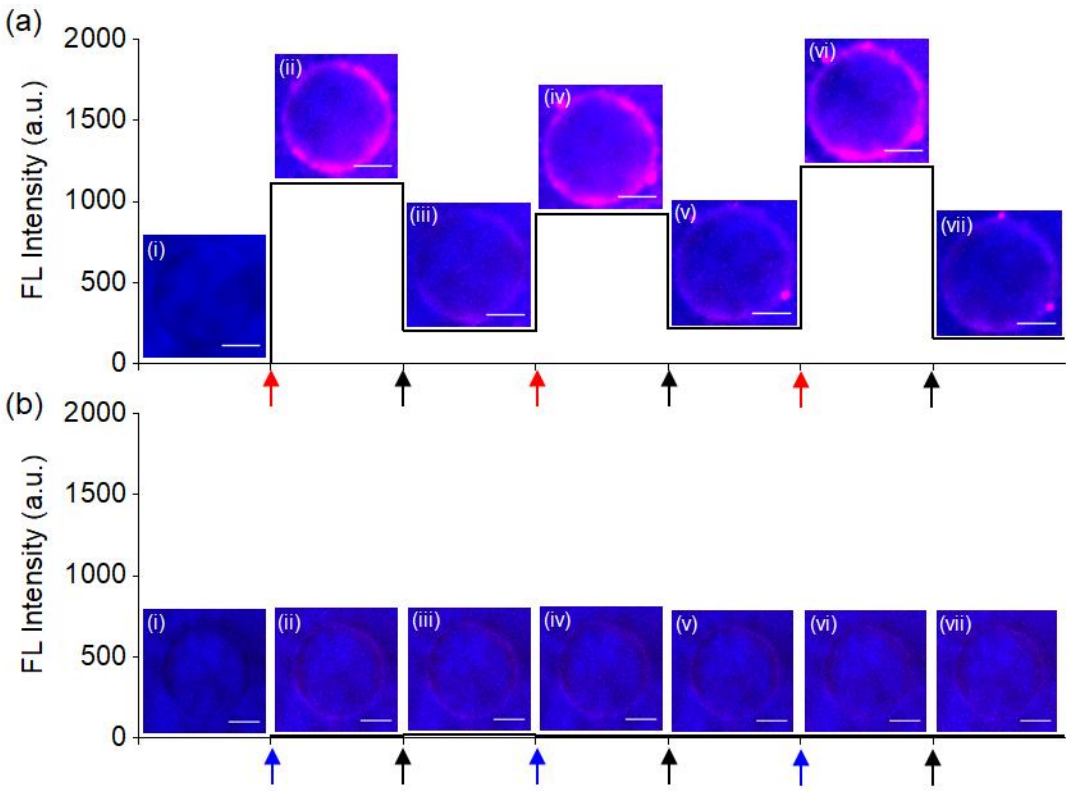

Figure 4.10. Reversible vesicle aggregation with DNA signals. (a) Fluorescence intensity of the small vesicles around the GUV on each experimental step. Corresponding images of fluorescence overlaid on brightfield images are also presented. Oligonucleotides (red strands in Figure 1) and rhodamine B dyes are present in the SUVs for imaging. On its surface, the giant vesicle includes DNA strands (blue strands in Figure 1), but does not have DNA origami pores or particles of polystyrene. (i) A giant vesicle is immobilized through biotin-streptavidin conjugation in the microfluidic imaging chamber. (ii) The introduction of small vesicles and 36-nt SUV-linker DNA (indicated by the red arrow) will cause SUV clustering on the giant vesicle through the base pairing of the giant and small vesicle linkers with the strands. The fluorescence intensity increases significantly as a result. (iii) A collection of SUV release strands, represented by a black arrow, is given. First the signaling oligonucleotides can bind with the 6-nt toehold and completely hybridize with the SUV-linkers, thus eliminating the vesicle linkers. Thus the tiny vesicles can dissociate from the GUV, and the strength of fluorescence decreases dramatically. (iv)—The (vii). With DNA signals, you can repeat the reversible vesicle aggregation (SUV linkers and releasers). (b) Control experiment, using a random sequence of DNA rather than the SUV linkers (represented by the blue arrows). As predicted, the small vesicles are not attached to the GUV, so no major fluorescence changes have been observed. Scale bars are 5 μm in all images.

Reversible aggregation behavior using hairpin signal

Finally, we demonstrated the recognition and transduction of DNA signals through membrane pores for programmable vesicle aggregation. Here we used the 56-nt hairpin that contains complementary domains for the strands on the vesicles (*i.e.*, SUV linker sequence). As discussed

in Figure 4.1, the domains are initially shielded so that aggregation cannot be directly induced (Figure 4.11). To reveal the SUV-linker domain via enzymatic digestion, this hairpin signal can be transduced by Exo III. During the assembly, the Exo III-modified, fluorescein-labeled polystyrene particles were encapsulated in the great vesicle. The enzyme-particles are too large to pass through the DNA origami pores, thus they float randomly inside the GUV, shown as yellow dots in the fluorescence image in Figure 4.11a. Using this large vesicle with the DNA pores initially closed by flat origami caps (state I signal recognition and transduction were demonstrated. As indicated by the orange arrow, we first opened the DNA pores with the cap releasers (state (ii)). Via membrane channels, the hairpins will then join the vesicle and interact with Exo III enzymes so that the shielding domain is cut off and the 36-nt SUV-linker signal is exposed. They can bind with the oligonucleotides on the tiny and wide vesicles when the SUV linkers move out of the GUV. As a consequence, the GUV aggregates the SUVs, showing the pattern of circular fluorescence around the large vesicle (state (iii)). Then, when the SUV releasers were added (indicated by black arrows), the clustered, small vesicles were dissociated (state (iv)), similar to what is seen in Figure 4.10. This programmable clustering has been replicated twice and can be cycled continuously as long as new DNA signals are given and the chemical waste is removed. We have substituted the hairpin strand with a random series as a control experiment. As expected, the small vesicles did not accumulate on the GUV, with no noticeable fluorescence change noted (Figure 4.11b). It is noteworthy that, as shown in Figure 4.11a and Figures 4.6 and 4.13, the shape of immobilized vesicles may change slightly over time. It is also clear that the fluorescence becomes very small with the release signals, but it does not drop to 0 (Figure 4.11a). Any nonspecific attachment of small vesicles can be due to this. Nonetheless, our experiment clearly shows the efficacy of DNA signals in artificial cells' programming aggregation behaviors.

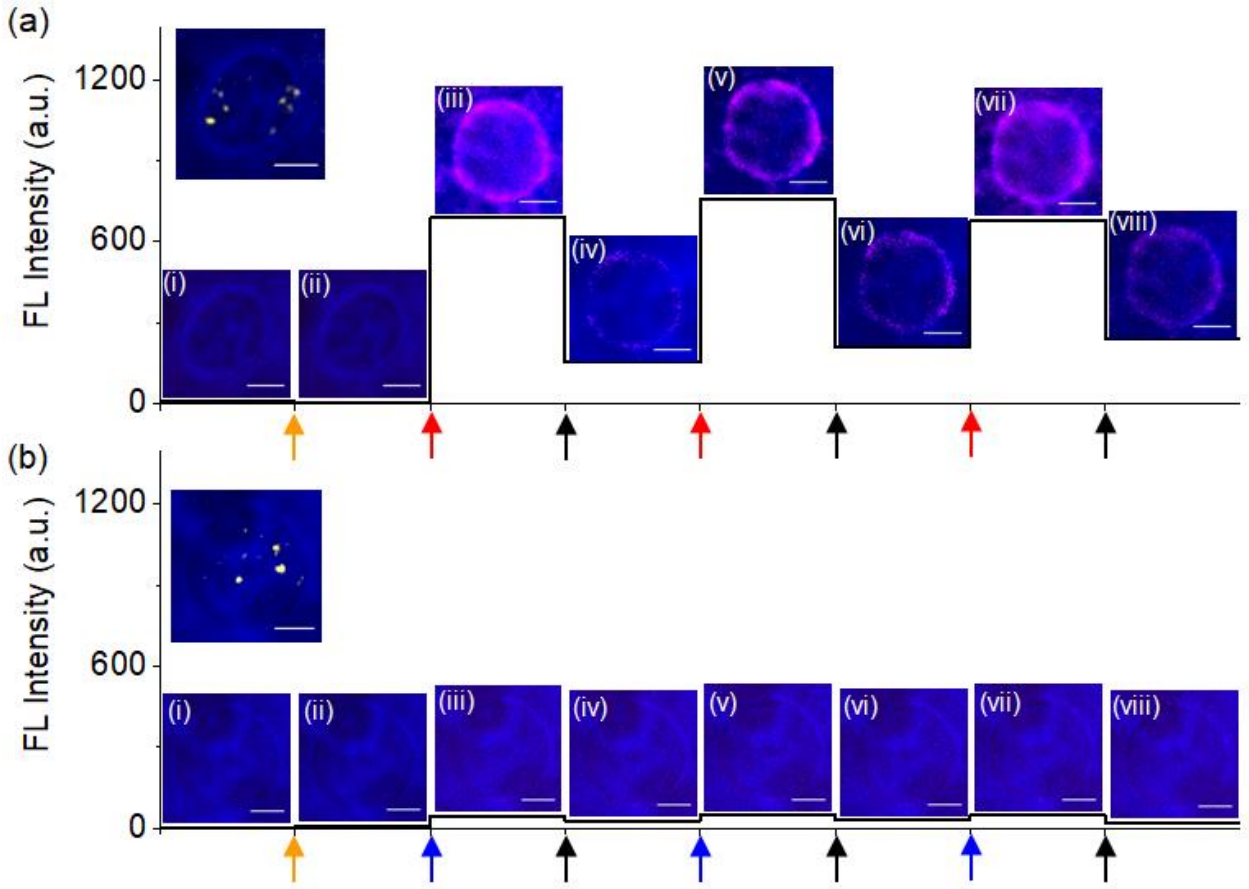

Figure 4.11. (a) Dynamic aggregation behavior of artificial cells programmed by Hairpin signals. To receive and transmit signals, tubular origami pores are included in the giant vesicle which also encapsulates Exo-III modified polystyrene particles. The 200-nm-diameter particles, seen in the upper left image as yellow dots, float randomly within the GUV. I In the imaging chamber, a giant vesicle is immobilized. (ii) To remove the flat origami caps, a collection of cap releaser strands are given (orange arrow). (iii) As the red arrow shows, the hairpin strands and small vesicles are added to the tube. The hairpins penetrate through the transmembrane origami channels into the vesicle and are partially digested by Exo III, revealing the domain of the SUV linker. On the small and large vesicles, the transduced oligonucleotides diffuse out through the pores and bind with the strands. As a result, the tiny vesicles cluster around the surface of the GUV, which is apparent with a circular fluorescent image superimposed on the giant vesicle's bright field image. (iv) When the SUV releasers (represented by the black arrow) are inserted, the SUV linkers are removed by means of a toehold-mediated displacement of the strand. Then the tiny vesicles dissociate from the GUV, and the intensity of the fluorescence decreases dramatically. (v)-(viii) You can replicate the programmable clustering action of DNA many times. (b) Use a random series instead of a hairpin to monitor the experiment. (i)-(ii) The opening of the DNA pores is achieved by removing the caps (indicated by the orange arrow). (iii) Random sequence oligonucleotides may join the giant vesicle (blue arrow), but they are unable to cause small vesicle aggregation at the GUV. Therefore, no major fluorescence variations have been observed (iii). (iv) No modifications in the actions of the vesicles would result from the addition of SUV releasers. Scale bars are 5 μm in all images.

Additional aggregation experiments using hairpin strand

The reversible aggregation experiment using the SUV linkers was more efficient than using the hairpin strands because it skips the process of (i) pore opening, (ii) hairpin penetration into the vesicle, (iii) cleavage by Exo III, and (iv) outflow of the transduced oligonucleotides (*i.e.*, exposed SUV linkers) from the GUV. Therefore, we observed a more drastic change in fluorescence intensity in less amount of time. In the aggregation experiment using SUV linkers, approximately 30 mins were given for the SUVs to aggregate onto the giant vesicle. About 20 mins were given for the small vesicles to dissociate from the GUV. However, with the hairpin strands, an hour was given for each step during the course of experiment. Figures 4.12 and 4.13 present additional reversible aggregation experiments (similar to Figure 4.11). To confirm that the hairpin strand itself cannot trigger the aggregation, we performed a control experiment that did not include the first step of adding cap releaser strands. Without cap releasers, the origami channels on the giant vesicles remain closed with the rectangular origami caps. As a result, SUVs and hairpins cannot initiate the aggregation of small vesicles on the giant vesicle, as shown in Figure 4.14.

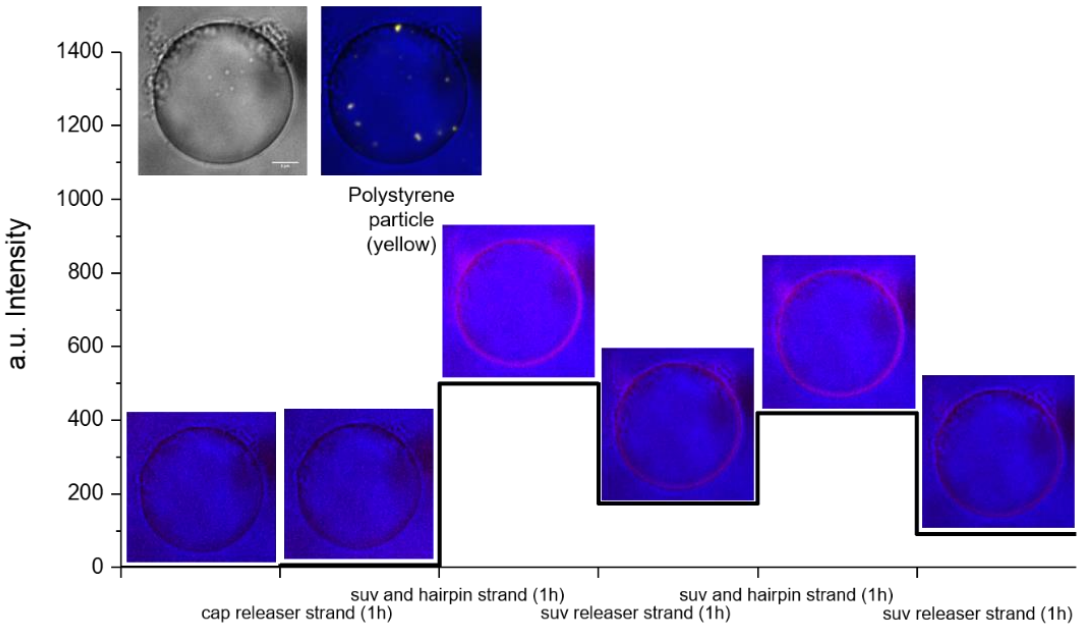

Figure 4.12. Additional reversible aggregation experiment with 2 cycles of adding SUVs, hairpin strands, and SUV releasers. For each step, we kept 1-hour incubation time, because the change of fluorescence intensity gradually stopped after 40 to 50 mins. Similar to Figure 5, yellow dots in the top left image represents polystyrene particles functionalized with Exo III enzymes. Circular fluorescence ring indicates the aggregation of small vesicles on the surface of the giant vesicle.

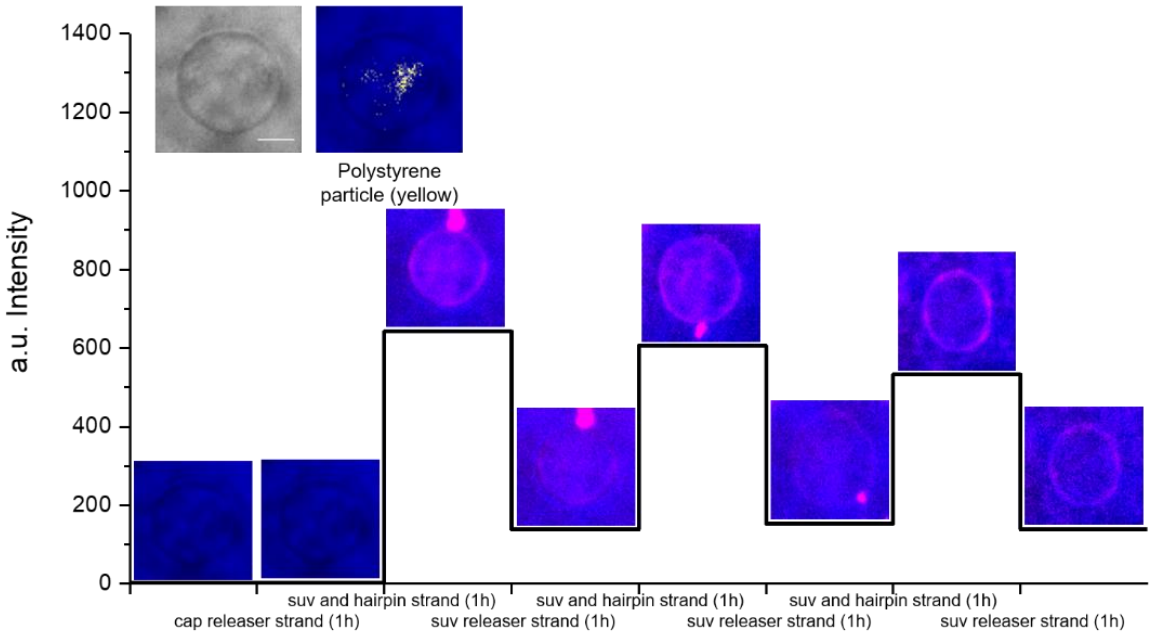

Figure 4.13. Additional aggregation experiment with hairpin signals. Significant changes of fluorescence intensity were observed during the course of experiment. It is noticeable that the GUV immobilized on the glass surface gradually changed its shape from a sphere to ellipsoid. We suspect that this might be caused by the flow in the microfluidic channel.

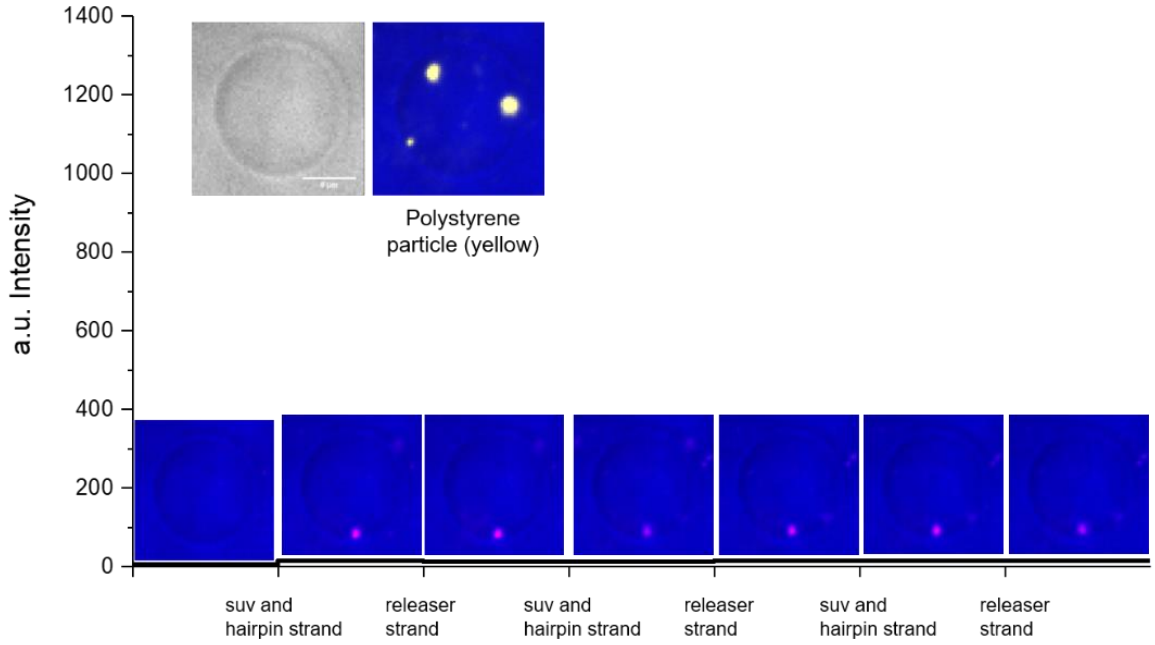

Figure 4.14. Control experiment without cap releaser strands. Small vesicles and hairpin strands were introduced into the microfluidic imaging chamber where a giant vesicle was immobilized with DNA pores closed with origami caps. Without adding cap releaser strands, the origami channels on the GUV remained closed; therefore, hairpin strands could not enter the GUV to become active SUV linker strand. As a result, we did not observe significant SUV binding on the GUV. There is only one spot that has nonspecifically bound SUV which was not removed by the SUV releaser strand.

4.5 Conclusion

In this chapter, we have shown chemical communication and cooperative behavior of synthetic cells using DNA signals. When and only when it was allowed to reach the cell via membrane channels and interact with enzymes, the main hairpin signal was successful for the purpose. Biochemical signals were essential for receiving, transducing and transmitting the DNA origami-based transmembrane channels. Interaction between vesicles following DNA signals demonstrates tremendous potential for multi-cellular activities that are more complex. This study will help build synthetic cells for cell biology and neuroscience research as a surrogate model. For instance, to research mechanisms for transmitting and receiving neurotransmitters, an artificial neuronal network could be built. Such a forum could elucidate sensation transmission mechanisms such as pain, which have historically been hard to research. Overall, we expect the growing DNA nanotechnology tool library to open up new opportunities for both fundamental sciences and novel applications in biotechnology.

5. CONCLUSION AND FUTURE WORK

5.1 Conclusion

In this thesis, DNA is studied for applications in aggregation and fusion behaviors of synthetic cells. Mechanisms and kinetics of DNA signal induced cell fusion and aggregation have been studied. With the help of DNA nanotechnology, it is possible to achieve chemical communication and cooperative behavior of synthetic cells, as well as construct a DNA origami transmembrane channel for receiving, transducing, and transmitting biochemical signals.

In the artificial cell system, DNA signals are proven to trigger liposome fusion and reversible liposome aggregation and release. DNA has been used for the combination of all its properties, including liposome linking and releasing, Exo III digestion, and DNA origami pore construction. With the demonstration of using DNA signals to control the artificial cell systems, it may also be possible to use DNA strands to control real cells.

DNA as an engineering material has been explored far beyond its traditional genetic carrier function with these studies. In fact, building on the fundamental DNA base pairing property, DNA nanotechnology has developed dramatically. Starting from the very simple DNA structure formed by several single-strand DNA, complex 2-D or 3-D structures have been constructed by DNA. These structures could even achieve certain functions interacting with different systems. DNA nanotechnology affected research area has been broader and broader. As the research work keeps progressing forward, it will be closer and closer to using DNA signals, either synthesized or natural to interact with the live system for better understanding and control.

5.2 Future Work

Current research on DNA associated liposome research is quite limited. The majority of them are putting DNA strands on liposomes' surface and perform functions on that like liposome linking or fusion. However, the complex DNA structures such as DNA origami pores have not been explored much. As the research of artificial cells expands further, the synthetic cells will certainly become more complex. Powerful DNA nanostructures will be needed for artificial cell study. Thus,

improving the existing DNA origami pore system will be necessary. With the current DNA origami pore system, ON/OFF function can and should be added, with controlled by DNA signals and also involving other external signals including light, pH, heat and more.

The interaction between vesicles following DNA signals shows great potential for more complex multi-cellular behaviors. This study will help construct synthetic cells as a surrogate model system for cell biology and neuroscience research. For example, an artificial neuronal network could be constructed to study mechanisms for transferring and receiving neurotransmitters. Such a platform could elucidate propagation pathways of sensation such as pain, which has been traditionally difficult to study. Overall, we envision that the growing library of DNA nanotechnology tools will open new opportunities for both fundamental sciences and novel biotechnology applications.

REFERENCES

1 Seeman, N. C. & Sleiman, H. F. DNA Nanotechnology. *Nature Reviews Materials* **3**, 17068 (2017).

2 Chen, Y.-J., Groves, B., Muscat, R. A. & Seelig, G. DNA Nanotechnology from the Test Tube to the Cell. *Nature Nanotechnology* **10**, 748-760 (2015).

3 Kallenbach, N. R., Ma, R.-I. & Seeman, N. C. An Immobile Nucleic Acid Junction Constructed from Oligonucleotides. *Nature* **305**, 829-831 (1983).

4 Rothemund, P. W. K. Folding DNA to Create Nanoscale Shapes And Patterns. *Nature* **440**, 297-302 (2006).

5 Chang, T. Report on "Method for Preparing Artificial Hemoglobin Corpuscles". *Physiology McGill* (1957).

6 Xu, C., Hu, S. & Chen, X. Artificial Cells: from Basic Science to Applications. *Materials Today* **19**, 516-532 (2016).

7 Jia, H. & Schwille, P. Bottom-Up Synthetic Biology: Reconstitution in Space And Time. *Current Opinion in Biotechnology* **60**, 179-187 (2019).

8 Göpfrich, K., Li, C.-Y., Ricci, M., Bhamidimarri, S. P., Yoo, J., Gyenes, B., Ohmann, A., Winterhalte, M., Aksimentiev, A. & Keyser, U. F. Large-Conductance Transmembrane Porin Made From DNA Origami. *ACS Nano* **10**, 8207-8214 (2016).

9 Langecker, M., Arnaut, V., Martin, T. G., List, J., Renner, S., Mayer, M., Dietz, H. & Simmel, F. C. Synthetic Lipid Membrane Channels Formed by Designed DNA Nanostructures. *Science* **338**, 932-936 (2012).

10 Ungermann, C. & Langosch, D. Functions of SNAREs in Intracellular Membrane Fusion And Lipid Bilayer Mixing. *Journal of Cell Science* **118**, 3819-3828 (2005).

11 Rampling, M. W., Meiselman, H. J., Neu, B. & Baskurt, O. K. Influence of Cell-Specific Factors on Red Blood Cell Aggregation *Biorheology* **41**, 91-112 (2004).

12 Toyoda, T., Mae, S.-I., Tanaka, H., Kondo, Y., Funato, M., Hosokawa, Y., Sudo, T., Kawaguchi, Y. & Osafune, K. Cell Aggregation Optimizes the Differentiation of Human ESCs and iPSCs into Pancreatic Bud-like Progenitor Cells. *Stem Cell Research* **14**, 185-197 (2015).

13 Allion, A., Baron, J.-P. & Boulange-Petermann, L. Impact of Surface Energy and roughness on cell Distribution and Viability. *Biofouling* **22**, 269-278 (2006).

14 Kaneko, K. & Yomo, T. Cell Division, Differentiation and Dynamic Clustering. *Physica* **75**, 89-102 (1994).

15 Norotte, C., Marga, F. S., Niklason, L. E. & Forgacs, G. Scaffold-Free Vascular Tissue Engineering Using Bioprinting. *Biomaterials* **30**, 5910-5917 (2009).

16 Howard, D., Buttery, L. D., Shakesheff, K. M. & Roberts, S. J. Tissue Engineering: Strategies, Stem Cells and Scaffolds. *Journal of Anatomy* **213**, 66-72 (2008).

17 Schmid-Schönbein, H. & Volger, E. Red-Cell Aggregation And Red-Cell Deformability in Diabetes. *Diabetes* **25**, 897-902 (1975).

18 Chiba, M., Miyazaki, M. & Ishiwata, S. Quantitative Analysis of the Lamellarity of Giant Liposomes Prepared by the Inverted Emulsion Method. *Biophysical Journal* **107**, 346-354 (2014).

19 Kirby, C. & Gregoriadis, G. Dehydration-Rehydration Vesicles: A Simple Method for High Yield Drug Entrapment in Liposomes. *Bio/Technology* **2**, 979-984 (1984).

20 Riaz, M. K., Riaz, M. A., Zhang, X., Lin, C., H.Wong, K., X.Chen, Zhang, G., Lu, A. & Yang, Z. Surface Functionalization and Targeting Strategies of Liposomes in Solid Tumor Therapy: A Review *International Journal of Molecular Sciences* **19**, 195 (2018).

21 Kaneda, Y. Virosomes: Evolution of the Liposome as a Targeted Drug Delivery System. *Advanced Drug Delivery Reviews* **43**, 197-205 (2000).

22 Yang, J., Bahreman, A., Daudey, G., Bussmann, J., Olsthoorn, R. C. L. & Kros, A. Drug Delivery via Cell Membrane Fusion Using Lipopeptide Modified Liposomes. *ACS Central Science* **2**, 621-630 (2016).

23 Chen, E. H., Grote, E., Mohler, W. & Vignery, A. Cell–Cell Fusion. *FEBS Letters* **581**, 2181-2193 (2007).

24 Löffler, P. M. G., Ries, O., Rabe, A., Okholm, A. H., Thomsen, R. P., Kjems, J. & Voge, S. A DNA-Programmed Liposome Fusion Cascade. *Angewandte Chemie International Edition* **56**, 13228-13231 (2017).

25 Stengel, G., Zahn, R. & Höök, F. DNA-induced Programmable Fusion of Phospholipid Vesicles. *Journal of the American Chemical Society* **129**, 9584-9585 (2007).

26 Chan, Y.-H. M., Lengerich, B. V. & Boxer, S. G. Effects of Linker Sequences on Vesicle Fusion Mediated by Lipid-Anchored DNA Oligonucleotides. *Proceedings of the National Academy of Sciences of the United States of America* **106**, 979-984 (2009).

27 Saltzman, W. M. & Kyriakides, T. R. *Cell Interactions with Polymers*. 385-406 (2014).

28 Bridges, A. B., Hill, A. & Belch, J. J. Cigarette Smoking Increases White Blood Cell Aggregation in Whole Blood. *Journal of the Royal Society of Medicine* **86**, 139-140 (1993).

29 Pessac, B. & Defendi, V. Cell Aggregation: Role of Acid Mucopolysaccharides. *Science* **175**, 898-900 (1972).

30 Pan, J., Du, Y., Qiu, H., Upton, L. R., Li, F. & Choi, J. H. Mimicking Chemotactic Cell Migration with DNA Programmable Synthetic Vesicles. *Nano Letters* **19**, 9138-9144 (2019).

31 Jones, M. R., Seeman, N. C. & Mirkin, C. A. Programmable Materials and the Nature of the DNA Bond. *Science* **347**, 1260901 (2015).

32 Seeman, N. C. Nanomaterials Based on DNA. *Annual Review of Biochemistry* **79**, 65-87 (2010).

33 Pinheiro, A. V., Han, D., Shih, W. M. & Yan, H. Challenges and Opportunities for Structural DNA Nanotechnology. *Nature Nanotechnology* **6**, 763-772 (2011).

34 Sen, D. & Gilbert, W. A Sodium-potassium Switch in the Formation of Four-stranded G4-DNA. *Nature* **344**, 410-414 (1990).

35 Pan, J., Cha, T.-G., Li, F., Chen, H., Bragg, N. A. & Choi, J. H. Visible/near-infrared Subdiffraction Imaging Reveals the Stochastic Nature of DNA Walkers. *Science Advances* **3**, e1601600 (2017).

36 Liu, Q., Wang, L., Frutos, A. G., Condon, A. E., Corn, R. M. & Smith, L. M. DNA Computing on Surfaces. *Nature* **403**, 175-179 (2000).

37 Kurokawa, C., Fujiwara, K., Morita, M., Kawamata, I., Kawagishi, Y., Sakai, A., Murayama, Y., Nomura, S.-I. M., Murata, S., Takinoue, M. & Yanagisawa, M. DNA Cytoskeleton for Stabilizing Artificial Cells. *Proceedings of the National Academy of Sciences of the United States of America* **114**, 7228-7233 (2017).

38 Franquelim, H. G., Khmelinskaia, A., Sobczak, J.-P., Dietz, H. & Schwille, P. Membrane Sculpting by Curved DNA Origami Scaffolds. *Nature Communications* **9**, 811 (2018).

39 Burns, J. R., Seifert, A., Fertig, N. & Howorka, S. A Biomimetic DNA-based Channel for the Ligand-controlled Transport of Charged Molecular Cargo Across a Biological Membrane. *Nature Nanotechnology* **11**, 152-156 (2016).

40 Bell, N. A. W., Engst, C. R., Ablay, M., Divtini, G., Ducati, C., Liedl, T. & Keyser, U. F. DNA Origami Nanopores. *Nano Letters* **12**, 512-517 (2012).

41 Burns, J. R., Göpfrich, K., Wood, J. W., Thacker, V. V., Stulz, E., Keyser, U. F. & Howorka, S. Lipid-bilayer-spanning DNA Nanopores with a Bifunctional Porphyrin Anchor. *Angewandte Chemie International Edition* **52**, 12069-12072 (2013).

42 Krishnan, S., Ziegler, D., Arnaut, V., Martin, T. G., Kapsner, K., Henneberg, K., Bausch, A. R., Dietz, H. & Simmel, F. C. Molecular Transport Through Large-diameter DNA Nanopores. *Nature Communications* **7**, 12787 (2016).

43 Thomsen, R. P., Malle, M. G., Okholm, A. H., Krishnan, S., Bohr, S. S.-R., Sørensen, R. S., Ries, O., Vogel, S., Simmel, F. C., Hatzakis, N. S. & Kjems, J. A Large Size-selective DNA Nanopore with Sensing Applications. *Nature Communications* **10**, 5655 (2019).

44 Choi, J., Chen, H., Li, F., Yang, L., Kim, S. S., Naik, R. R., Ye, P. D. & Choi, J. H. Nanomanufacturing of 2D Transition Metal Dichalcogenide Materials Using Self-Assembled DNA Nanotubes. *Small* **11**, 5520-5527 (2015).

45 Li, F., Chen, H., Pan, J., Cha, T.-G., Medintz, I. L. & Choi, J. H. A DNAzyme-mediated Logic Gate for Programming Molecular Capture and Release on DNA origami. *Chemical Communications* **52**, 8369-8372 (2016).

46 Douglas, S. M., Dietz, H., Liedl, T., Högberg, B., Graf, F. & Shih, W. M. Self-assembly of DNA into Nanoscale Three-dimensional Shapes. *Nature* **459**, 414-418 (2009).

47 Bayley, H. Designed Membrane Channels and Pores. *Current Opinion in Biotechnology* **10**, 94-103 (1999).

48 Ketterer, P., Ananth, A. N., Trip, D. S. L., Mishra, A., Bertosin, E., Ganji, M., Torre, J. V. D., Onck, P., Dietz, H. & Dekker, C. DNA Origami Scaffold for Studying Intrinsically Disordered Proteins of the Nuclear Pore Complex. *Nature Communications* **9**, 902 (2018).

49 Srinivas, N., Ouldridge, T. E., Šulc, P., Schaeffer, J. M., Yurke, B., Louis, A. A., Doye, J. P. K. & Winfree, E. On the Biophysics and Kinetics of Toehold-mediated DNA Strand Displacement. *Nucleic Acids Research* **41**, 10641-10658 (2013).

50 Chen, H., Wang, T.-W., Riccitelli, M. M., Cui, Y., Irudayaraj, J. & Choi, J. H. Understanding the Mechanical Properties of DNA Origami Tiles and Controlling the Kinetics of Their Folding and Unfolding Reconfiguration. *Journal of the American Chemical Society* **136**, 6995-7005 (2014).

APPENDIX A. ORIGAMI SEQUENCE

Table A.1. Blue and gray staple sequences for the origami tile shown in Figure 4.2. Colored parts correspond to the colored dots in Figure 4.2. For example, staple [02,08] in Figure 4.2a has a red dot. In this table, there is a red '/5Cy5/' at the 5' end of the staple's sequence. Similar notations apply to pink (pore-cap connection) and green (cap-pore connection) colored parts. For the staple without a colored dot, colored parts will not show up in the sequence. This means that staple [02,08] in Figure 4.2b does not have '/5Cy5/' at the 5' end.

Blue staples		Gray staples	
Name	Sequence	Name	Sequence
[02, 04]	TGTCACTCTGTCCGAAGAACGGTACAGAACAATATTACCGAATACCTA	[03, 05]	GTAATATCCGCCAGAATCCTGAGAGTATAACG
[02, 08]	/5Cy5/TATAATCAGAACTCAAACTATCGGATGGATTA	[03, 09]	GAGTAGAAGTGAGGCCACCGAGTAGAGCGGGC
[02, 12]	TGTCCATCGATTAGTAATAACATCACACGACC	[03, 17]	AAAATCCCTGAGTGTTGTTCCAGTCGATTTAG
[02, 20]	AGAGTCCATTTGATGGTGGTTCCGAGAGGCGG	[03, 21]	AAATCCTGCTATTAAAGAACGTGGAAGCACTA
[02, 24]	GTCAAAGGACGCTGGTTTGCCCCATTTTTCTT	[03, 25]	TGTCACTCTGTCCGAAAGCGGTCCGCGAAAAACCGTCTATCAAATCAA
[04, 04]	TGTCACTCTGTCCGAACATTTTGAATGCGCGAACTGATAGAACCACCA	[05, 05]	AGTCTTTACGCTCAATCGTCTGAACCTTGCTG
[04, 08]	TTTACATTAGACAATATTTTTGAACGGTCAGT	[05, 09]	CGTGGCACGGCAGATTCACCAGTCACTTGCCT
[04, 12]	AGTAATAATTCTGACCTGAAAGCGACGCTGAG	[05, 17]	TCCAGTCGCGGCCAACGCGCGGGGAAATCGGC
[04, 20]	TTTGCGTATTGCGTTGCGCTCACTGGGTACCG	[05, 21]	CACATTAATTGGGCGCCAGGGTGGGCAGGCGA
[04, 24]	TTCACCAGGGGTGCCTAATGAGTGTAGCTGTT	[05, 25]	TGTCACTCTGTCCGAAAAAGCCTGTGAGACGGGCAACAGCTTGCAGCA
[06, 04]	TGTCACTCTGTCCGAAGCAGAAGATGAGGAAGGTTATCTATTAGAGCC	[07, 05]	AAAGGAATTAAAACAGAGGTGAGGTGGCTATT
[06, 08]	ATTAACACGGTCAGTTGGCAAATCTTTAGAAG	[07, 09]	CAATATCTCGCCTGCAACAGTGCCTAAGAATA
[06, 12]	AGCCAGCAAACCTCAAATATCAAACAACTCGT	[07, 17]	AAAACGACACTCTAGAGGATCCCCGCCCGCTT
[06, 20]	AGCTCGAAGGGTTTTCCCAGTCACTCTGGTGC	[07, 21]	TAACGCCATTCGTAATCATGGTCAAGCTAACT
[06, 24]	TCCTGTGTGTGCTGCAAGGCGATTGCCATTCA	[07, 25]	TGTCACTCTGTCCGAAAGGGGGATGAAATTGTTATCCGCTTAAAGTGT
[08, 04]	TGTCACTCTGTCCGAAGTCAATAGCTGATTATCAGATGATATTATACT	[09, 05]	TCATATTCATAATACATTTGAGGAAACAGTTG

[08, 08]	TATTAGACCCACCAGAAGGAGCGGCTACCATA	[09, 09]	CAAAGAAATTTACAAACAATTCGACCCTCAAT
[08, 12]	ATTAAATCGAGTAACATTATCATTGAAATAAA	[09, 17]	CGACGACAGCTTTCCGGCACCGCTGACGTTGT
[08, 20]	CGGAAACCCGTGCATCTGCCAGTTTAATTCGC	[09, 21]	ATCGTAACAGGCAAAGCGCCATTCAAGTTGGG
[08, 24]	GGCTGCGCGGTCACGTTGGTGTAGTCATCAAC	[09, 25]	TGTCACTCTGTCCGAAATGGGATAAACTGTTGGGAAGGGCCTGGCGAA
[10, 04]	TGTCACTCTGTCCGAATCTGAATAAAGTTACAAAATCGCGCAAAAGAA	[11, 05]	TGAATACCATGGAAGGGTTAGAACAATTATCA
[10, 08]	TCAAAATTAATAACGGATTCGCCTACAAAATT	[11, 09]	GGAGAAACATTTGCACGTAAAACATTGCGGAA
[10, 12]	GAAATTGCACAGTAACAGTACCTTAATTACCT	[11, 17]	AGTGCTGATTCGGACAGAGTGACACATTAAATGGAACGCCATCAAAAATGAGGGGA
[10, 20]	GTCTGGCCACGTTAATATTTTGTTGGTCATTG	[11, 21]	AATTGTAATTCCTGTAGCCAGCTTATGGGCGC
[10, 24]	ATTAAATGGAAGATTGTATAAGCAGAATCGAT	[11, 25]	TGTCACTCTGTCCGAAAAAAACAGTGAGCGAGTAACAACCTGACCGTA
[12, 04]	TGTCACTCTGTCCGAAGATGATGAGCGATAGCTTAGATTAAAAATCAT	[13, 05]	AAAACATAAACAAACATCAAGAAAGATTGCTT
[12, 08]	AATTACATATTAATTTTCCCTTAGCCTCCGGC	[13, 09]	AGTGCTGATTCGGACAGAGTGACACGCTATTATTAACAATTTCATTTGTTACATCG
[12, 12]	AGTGCTGATTCGGACAGAGTGACATTTTTAATAATAACCTTGCTTCTGGTAAATGC	[13, 17]	TGATAAATTCTACAAAGGCTATCAAAAATTCG
[12, 20]	AGTGCTGATTCGGACAGAGTGACACCTGAGAGAATATGATATTCAACCTAATACTT	[13, 21]	TCACCATCTCTGGAGCAAACAAGAAATATTTA
[12, 24]	GAACGGTATGAGAAAGGCCGGAGACGCAAGGA	[13, 25]	TGTCACTCTGTCCGAACAAAAGGGATCGTAAAACTAGCATAAAGCCCC
[14, 04]	TGTCACTCTGTCCGAAAGGTCTGACGTGTGATAAATAAGGTACTAGAA	[15, 05]	ATACCGACGAGACTACCTTTTTAAAATCCTTG
[14, 08]	TTAGGTTGCTGACCTAAATTTAATTTATACAA	[15, 09]	TTCATCTTGGTTATATAACTATATTAAATCGT
[14, 12]	TGATGCAATTTTTCAAATATATTTCTCAACAG	[15, 17]	AATAAAGCAAACATTATGACCCTGGTTCTAGC
[14, 20]	TTGCGGGAGGCAAAGAATTAGCAAGTAGATTT	[15, 21]	ACAGGCAAGAAGCCTTTATTTCAACAGTCAAA
[14, 24]	TAAAAATTTAGCATTAACATCCAACAAATGGT	[15, 25]	TGTCACTCTGTCCGAAAATAGTAGTTTAGAACCCTCATATTAAAGATT
[16, 04]	TGTCACTCTGTCCGAAAAAGCCTGAAAGTAATTCTGTCCAGCAGAACG	[17, 05]	CAAAAGGTTTTAGTATCATATGCGGGTTTGAA
[16, 08]	ATTCTTACTAATAAGAGAATATAAGTCCTGAA	[17, 09]	AGTGCTGATTCGGACAGAGTGACACGAGCCAGCAGTATAAAGCCAACGTAGTTAAT
[16, 12]	TAGGGCTTATGTAATTTAGGCAGAATTTACGA	[17, 17]	TACGGTGTCCAATTCTGCGAACGAAATTAAGC

[16, 20]	AGTTTGACCATGTTTTAAATATGCTAATTCGA	[17, 21]	AGTGCTGATTCGGACAGAGTGACATAGCTCAACATTAGATACATTTCGTAAATCAT
[16, 24]	CAATAACCGCTTAATTGCTGAATAGCAAACTC	[17, 25]	TGTCACTCTGTCCGAAGGCTTAGATGTTTAGCTATATTTTATTCTACT
[18, 04]	TGTCACTCTGTCCGAACGCCTGTTTTCATCGTAGGAATCAAGAAGGCT	[19, 05]	TTTTTATTTATCAACAATAGATAAAGTACCGA
[18, 08]	CAAGAAAACACTCATCGAGAACAAGCGTTTTA	[19, 09]	AGTGCTGATTCGGACAGAGTGACAAAGTACCGATAATATCCCATCCTAGGCATTTT
[18, 12]	GCATGTAGCATTCCAAGAACGGGTTTTTGAAG	[19, 17]	GCGGATTGTTCAAATATCGCGTTTAACTAAAG
[18, 20]	GCTTCAAACTGACTATTATAGTCAGCCAGAGG	[19, 21]	TCTTTACCGCGAACCAGACCGGAATAATGCTG
[18, 24]	CAACAGGTAATGACCATAAATCAAGGATAGCG	[19, 25]	TGTCACTCTGTCCGAAAAAACGAGCAGGATTAGAGAGTACTTGCGGAT
[20, 04]	TGTCACTCTGTCCGAATATCCGGTAATAAACAGCCATATTTGTTTAAC	[21, 05]	AGTTACAAATTCTAAGAACGCGAGGCAAGCCG
[20, 08]	GCGAACCTCGTCTTTCCAGAGCCTTACAGAGA	[21, 09]	CTAACGAGCCCGACTTGCGGGAGGATTAAACC
[20, 12]	CCTTAAATATTTTATCCTGAATCTCATTAGAC	[21, 17]	TTTACCAGTTGCAAAAGAAGTTTTGAAGCAAA
[20, 20]	AGTGCTGATTCGGACAGAGTGACAGGGTAATAAGAGCAACACTATCATCGTTGGGA	[21, 21]	GCATAGTAGTAAAATGTTTAGACTAAATCAGG
[20, 24]	TCCAATACCATAACGCCAAAAGGAAACTAACG	[21, 25]	TGTCACTCTGTCCGAATGCAGATATGCGGAATCGTCATAACAGTTCAG
[22, 04]	TGTCACTCTGTCCGAAGTCAAAAAAAACAATGAAATAGCAAGTAAGCA	[23, 05]	AGAGCAAGTGAAAATAGCAGCCTTAATTTGCC
[22, 08]	GAATAACAAGAATTGAGTTAAGCCGGAAACCG	[23, 09]	AACCCACATAAAAACAGGGAAGCGTACCAACG
[22, 12]	AGTGCTGATTCGGACAGAGTGACAGGGAGAATATTGAGCGCTAATATCCCCAAAAG	[23, 17]	AGTGCTGATTCGGACAGAGTGACAATCATTGTATTATACCAGTCAGGAAACCCTCG
[22, 20]	AGAAAAATTGAGATGGTTTAATTTGGCGCATA	[23, 21]	ATTGGGCTCTACGTTAATAAAACGATTACGAG
[22, 24]	GAACAACAGAGAAACACCAGAACGAATCTTGA	[23, 25]	TGTCACTCTGTCCGAAGCCCTGACTTATTACAGGTAGAAATCAACTAA
[24, 04]	TGTCACTCTGTCCGAAGATAGCCGTAAGTTTATTTTGTCAGCCAAAGA	[25, 05]	CCACGGAAAACAAAGTTACCAGAACAATAATA
[24, 08]	AGGAAACGACATATAAAAGAAACGGAGGGAGG	[25, 09]	AGGTGGCACAATAATAACGGAATAAGAGAGAT
[24, 12]	AACTGGCACAAACGTAGAAAATACTTCATTAA	[25, 17]	TAAGGGAAAACGGTGTACAGACCACAACTTTA
[24, 20]	GGCTGGCTGAACGAGGCGCAGACGCGAAAGAG	[25, 21]	CTTAGCCGGACCTTCATCAAGAGTAGTAGTAA
[24, 24]	CAAGAACCAAATCCGCGACCTGCTATCTTTGA	[25, 25]	TGTCACTCTGTCCGAATTGTGTCGGGATATTCATTACCCATAAGGCTT

[26, 04]	TGTCACTCTGTCCGAACAAAAGGGAACCATCGATAGCAGCCTTTAGCG	[27, 05]	ACCAATGACGACATTCAACCGATTCAAAGACA
[26, 08]	GAAGGTAAACCATTAGCAAGGCCGGCATTTTC	[27, 09]	GCACCATTATATTGACGGAAATTAATACATAA
[26, 12]	AGGTGAATTTAGAGCCAGCAAAATTGCCATCT	[27, 17]	AGTTTCCAAGGCACCAACCTAAAAGTCAATCA
[26, 20]	GCAAAAGAGGACTAAAGACTTTTTTGACAACA	[27, 21]	GGCTTTGAATACACTAAAACACTCCCATGTTA
[26, 24]	CCCCCAGCAACGAGGGTAGCAACGTATTCGGT	[27, 25]	TGTCACTCTGTCCGAAAGCATCGGGATTATACCAAGCGCGCTGATAAA
[28, 04]	TGTCACTCTGTCCGAATCAGACTGCCACCAGAACCACCACGGCAGGTC	[29, 05]	CAGAGCCGTAGCGCGTTTTCATCGGAAACGTC
[28, 08]	GGTCATAGCGCCACCCTCAGAGCCAACAAATA	[29, 09]	CTCAGAACCCCCCTTATTAGCGTTCACCAGTA
[28, 12]	TTTCATAAACCGCCTCCCTCAGAGAAGCGCAG	[29, 17]	GCTTGCTTATAGTTGCGCCGACAACATGAGGA
[28, 20]	ACCATCGCGCCTTTAATTGTATCGTTAGTAAA	[29, 21]	CAAAAGGACCACGCATAACCGATAGCTACAGA
[28, 24]	CGCTGAGGTGAAAATCTCCAAAAATAAACAAC	[29, 25]	TGTCACTCTGTCCGAATTTCACGTCTTGCAGGGAGTTAAACGAAAGAC
[30, 04]	TGTCACTCTGTCCGAAAGACGATTCGTATAAACAGTTAATAAACATGA	[31, 05]	ACAGTGCCGGCCTTGATATTCACAACCACCCT
[30, 08]	AATCCTCATTAACGGGGTCAGTGCCAAGAGAA	[31, 09]	AATAAGTTTTAAAGCCAGAATGGACCGCCACC
[30, 12]	TCTCTGAATTGATGATACAGGAGTTCAGTACC	[31, 17]	ACAGACAGGTCGTCTTTCCAGACGGTTTATCA
[30, 20]	TGAATTTTAAACTACAACGCCTGTCACCGTAC	[31, 21]	ACCAGTACCTGTATGGGATTTTGCAAAGGCTC
[30, 24]	TTTCAACATGTACCGTAACACTGATCAGAACC	[31, 25]	TGTCACTCTGTCCGAAGGAACCCAGTTTCAGCGGAGTGAGAATAATTT

Table A.2. Red staple sequences for the origami tile shown in Figure 4.2. Sky-blue parts correspond to the sky-blue dots in Figure 4.2. For example, staple [02,16] in Figure 4.2a has a sky-blue dot. In this table, there is a sky-blue extension at the 3' end of the staple's sequence. All the sky-blue extensions are designed to bind with a cholesterol-DNA, whose sequence is TGGACGGCCGTCAACTGCGGCGTGTAA/3CholTEG/. For the staple without a sky-blue dot, colored parts will not show up in the sequence. This means, for example, that staple [02,16] in Figure 4.2b does not have the blue extension at the 3' end.

Red staples			
Name	Sequence	Name	Sequence
[02, 16]	GATAGGGTTTATAAATCAAAAGAAGTAGCAATTACACGCCGCAGTTGACGGCCGTCCA	[17, 13]	ACGCCAACAATTGAGAATCGCCATATATAACA
[03, 13]	ACTTCTTTACGCAAATTAACCGTTTAGCCCGA	[18, 16]	CGAAAGACCATCAAAAAGATTAAGGGCTGTCTTACACGCCGCAGTTGACGGCCGTCCA
[04, 16]	TAATGAATGGAAACCTGTCGTGCCAACAGAGATTACACGCCGCAGTTGACGGCCGTCCA	[19, 13]	TTCCTTATAAACCAATCAATAATCAGGAAGCC
[05, 13]	TAGAACCCAAGGGACATTCTGGCCAGCTGCAT	[20, 16]	AGAGGCTTACGACGATAAAAACCATTTGCACCTTACACGCCGCAGTTGACGGCCGTCCA
[06, 16]	GCAGGTCGGGCCAGTGCCAAGCTTAAGCATCATTACACGCCGCAGTTGACGGCCGTCCA	[21, 13]	CAGCTACACAAGATTAGTTGCTATAAATAGCG
[07, 13]	CCTTGCTGGCAAATGAAAAATCTAGCATGCCT	[22, 16]	ACTGGCTCGAATTACCTTATGCGAACAAAGTCTTACACGCCGCAGTTGACGGCCGTCCA
[08, 16]	TCCAGCCAGTATCGGCCTCAGGAATTAATTTTTTACACGCCGCAGTTGACGGCCGTCCA	[23, 13]	AGAGGGTATAACTGAACACCCTGATTTTAAGA
[09, 13]	AAAAGTTTCTTTGCCCGAACGTTAGATCGCAC	[24, 16]	GACAGATGCCGAACTGACCAACTTTTACGCAGTTACACGCCGCAGTTGACGGCCGTCCA
[10, 16]	AACCAATATTTTGTTAAATCAGCTAACGTCAGTTACACGCCGCAGTTGACGGCCGTCCA	[25, 13]	TATGTTAGTGATTAAGACTCCTTATGAAAGAG
[11, 13]	ATGAATATGTAGATTTTCAGGTTTCATTTTTT	[26, 16]	CACTACGATTAAACGGGTAAAATATTGAGCCATTACACGCCGCAGTTGACGGCCGTCCA
[12, 16]	TTGAGAGATAATGCCGGAGAGGGTTCAATATATTACACGCCGCAGTTGACGGCCGTCCA	[27, 13]	TTTGGGAATATCACCGTCACCGACCGTAATGC
[13, 13]	TGTGAGTGGGAAACAGTACATAAAAGCTATTT	[28, 16]	TGATACCGTCGAGGTGAATTTCTTCAGAGCCATTACACGCCGCAGTTGACGGCCGTCCA
[14, 16]	TGTACCAACTCAGAGCATAAAGCTAAGAACGCTTACACGCCGCAGTTGACGGCCGTCCA	[29, 13]	CCACCGGATCAAAATCACCGGAACAAACAGCT
[15, 13]	GAGAAAACATCCAATCGCAAGACAAAATCGGT	[30, 16]	AAAGTTTTCCCTCATAGTTAGCGTGCGTCATATTACACGCCGCAGTTGACGGCCGTCCA
[16, 16]	GTTGATTCCTGGAAGTTTCATTCCATTTAACATTACACGCCGCAGTTGACGGCCGTCCA	[31, 13]	CATGGCTTTTTACCGTTCCAGTAAAACGATCT

Table A.3. Sequence of tubular staples. These staples are designed to bind the upper and lower boundaries of the origami tile together, thus forming a tubular pore.

Tubular staples			
Name	Sequence	Name	Sequence
[1,8]	AACAGGAGGGAACCTATTATTCTGGCCCCCTG	[32,25]	AAGTATTATCGTTAGAATCAGAGCTTAGACAG
[1,40]	TGCTTTCCAGAGGCTGAGACTCCTCTTGAGTA	[32,57]	GGATTAGGGCTGGCAAACGAGCACAGTGTTTT
[1,72]	GCTAGGGCATTAGCGGGGTTTTGCGTACTGGT	[32,89]	AGGCGGATGGGAAGAAAGCGAAAGAAAGAGTC
[1,104]	GAAAGGAAAAGTGCCGTCGAGAGGGTTGATAT	[32,121]	AAGTATAGGGGGAAAGCCGGCGAACGTGGCGA
[1,136]	AGCTTGACCCCGGAATAGGTGTATAGCATTCC	[32,153]	TCAGGAGGCCCTAAAGGGAGCCCCTTGGAACA
[1,168]	AATCGGAATTTAGTACCGCCACCCGTTTCGTC	[32,185]	GCCACCCTGGGTCGAGGTGCCGTAACTCCAAC
[1,200]	GTTTTTTGCAGAACCGCCACCCTCGCCCAATA	[32,217]	CACCCTCATACGTGAACCATCACCCAGGGCGA

VITA

Hengming Qiu obtained a bachelor's degree in Mechanical Engineering at Rutgers University. His master research in the School of Mechanical Engineering at Purdue University focuses on DNA nanotechnology and artificial cells.